Real-time dynamics of *Plasmodium* NDC80 reveals unusual modes of chromosome segregation during parasite proliferation

Mohammad Zeeshan[1], Rajan Pandey[1], David J.P. Ferguson[2], Eelco C. Tromer[3], Robert Markus[1], Steven Abel[4], Declan Brady[1], Emilie Daniel[1], Rebecca Limenitakis[5], Andrew R. Bottrill[6], Karine G. Le Roch[4], Anthony A. Holder[7], Ross F. Waller[3], David S. Guttery[8] and Rita Tewari[1*]

[1]School of Life Sciences, Queens Medical Centre, University of Nottingham, Nottingham, NG7 2UH, UK; [2]Nuffield Department of Clinical Laboratory Science, University of Oxford, John Radcliffe Hospital, Oxford OX3 9DU, UK, [3]Department of Biochemistry, University of Cambridge, Cambridge CB2 1QW, UK; [4]Department of Molecular, Cell and Systems Biology, University of California Riverside, Riverside, California, United States of America; [5]Institute of Cell Biology, University of Bern, Bern 3012, Switzerland; [6]School of Life Sciences, Gibbelt Hill Campus, University of Warwick, Coventry CV4 7AL, UK; [7]Malaria Parasitology Laboratory, The Francis Crick Institute, London, NW1 1AT, UK; [8]Leicester Cancer Research Centre, University of Leicester, Leicester, LE2 7LX, UK.

These authors contributed equally: Mohammad Zeeshan, Rajan Pandey

[*]For correspondence

Rita Tewari: rita.tewari@nottingham.ac.uk

Short title: Spatiotemporal Kinetochore dynamics in *Plasmodium*

Abstract

Eukaryotic cell proliferation requires chromosome replication and precise segregation to ensure daughter cells have identical genomic copies. The genus *Plasmodium,* the causative agent of malaria, displays some remarkable aspects of nuclear division throughout its lifecycle to meet some peculiar and unique challenges of DNA replication and chromosome segregation. The parasite undergoes atypical endomitosis and endoreduplication with an intact nuclear membrane and intranuclear mitotic spindle. To understand these diverse modes of Plasmodium cell division, we have studied the behaviour and composition of the outer kinetochore NDC80 complex, a key part of the mitotic apparatus that attaches the centromere of chromosomes to microtubules of the mitotic spindle. Using NDC80-GFP live-cell imaging in *Plasmodium berghei* we observe spatio-temporal changes dynamic changes during proliferation, including highly unusual kinetochore arrangements during sexual stages. We identify a divergent SPC24 component of the NDC80 complex, previously thought to be missing, and completing a canonical, albeit unusual, NDC80 complex structure. Altogether, our studies reveal the kinetochore as an ideal starting point towards understanding the non-canonical modes of chromosome segregation and cell division in *Plasmodium.*

Keywords:

Malaria, *Plasmodium*, kinetochore, NDC80 complex, chromosome segregation, atypical cell division, endomitosis, meiosis.

Summary Statement

The dynamic localization and protein complex of a kinetochore marker Ndc80 examined during proliferative stages of the malaria parasite life-cycle reveal unique modes of chromosome segregation.

Introduction

Mitosis and meiosis are fundamental processes in cell division that enable DNA replication and chromosome segregation, and allow eukaryotic organisms to proliferate, propagate and survive. During these processes, microtubular spindles form to facilitate an equal segregation of duplicated chromosomes to the spindle poles. Chromosome attachment to the spindle microtubules (MTs) is mediated by kinetochores, which are large multi-protein complexes assembled on the centromere located at the constriction point of sister chromatids (Cheeseman, 2014; McKinley and Cheeseman, 2016; Musacchio and Desai, 2017; Vader and Musacchio, 2017). Each sister chromatid has its own kinetochore, oriented to facilitate movement to opposite poles of the spindle apparatus. During anaphase, the spindle elongates and the sister chromatids separate, resulting in segregation of the two genomes during telophase. The NDC80 complex is a key component of the kinetochore that mediates its attachment to spindle MTs.. In most model organisms, it is member of the network of conserved Knl1, Mis12 and NDC80complexes (KMN) (McKinley and Cheeseman, 2016; Petrovic et al., 2016). The ~170-190 kDa Ndc80 complex has two globular domains at either end of a ~57 nm elongated coiled-coil, forming a dumb-bell shape. It is a heterotetramer comprising a 1:1:1:1 ratio of NDC80 (also known as HEC1 in humans), NUF2, SPC24 and SPC25 sub-complexed as two heterodimers: NDC80 with NUF2 and SPC24 with SPC25 (Ciferri et al., 2005; Farrell and Gubbels, 2014; Wei et al., 2005). The C-termini of the SPC24-SPC25 dimer anchor the complex to the kinetochore; whereas the NDC80-NUF2 dimer mediates plus-end MT binding through its calponin homology domain (CHD) (Alushin et al., 2010; Farrell and Gubbels, 2014; Sundin et al., 2011).

Malaria, caused by the apicomplexan parasite *Plasmodium* spp.*,* remains one of the most prevalent and deadly infectious diseases worldwide, with 219 million clinical cases and 435,000 deaths in 2017 (WHO, 2018). *Plasmodium* has several morphologically distinct proliferative stages during its life cycle that alternates between vertebrate host and mosquito vector (**Fig.1**) (Francia and Striepen, 2014; Sinden, 1991a; Sinden, 1991b). A malaria parasite-infected female anopheles mosquito inoculates haploid sporozoites into the mammalian host during a blood meal. Sporozoites travel through blood stream to the liver and infect hepatocytes, where the parasite replicates and develops and into a schizont. At the end of this exo-erythrocytic schizogony the host cell is ruptured to release haploid merozoites, which infect erythrocytes. In the intra-erythrocytic phase, an initial ring stage form develops through the trophozoite form into a schizont, where multiple rounds of asexual multiplication occur (erythrocytic schizogony). At the end of schizogony, host cell rupture releases further merozoites that infect new erythrocytes.

Following erythrocyte invasion, some parasites differentiate into male (micro) and female (macro) gametocytes to initiate the sexual phase of the life cycle, which occurs inside the mosquito. These haploid parasites are arrested at the G0/G1 phase of the cell cycle (Arnot and Gull, 1998). Following activation by mosquito ingestion, gametogenesis is initiated. Male gametogenesis is very rapid with three rounds of genome replication from 1N to 8N within 15 min after activation. At the end, eight motile microgametes are released while the female only gets activate and round up and egress out of the red cell membrane. rGametogenesis can be studied *in vitro* using a culture medium that mimics the mosquito midgut environment (Billker et al., 1998; Tewari et al., 2005).

After fertilisation the zygote differentiates into a motile ookinete. The ookinete invades the mosquito midgut wall where it develops into an oocyst. At this stage multiple rounds of endomitotic division occurs in a process similar to what is observed during schizogony, which is followed by cytokinesis to form thousands of motile sporozoites (Francia and Striepen, 2014; Gerald et al., 2011). The sporozoites are released from the oocyst and migrate to the mosquito's salivary glands for transmission to the vertebrate host.

The life cycle of *Plasmodium* is characterized by two unique processes of mitosis and a single stage of meiosis. The first mitotic process occurs during schizogony within mammalian hepatocytes and erythrocytes, and during sporogony in oocysts in the mosquito vector (Sinden, 1991a; Sinden, 1991b) (**Fig. 1 (A)**). This mitotic division is atypical, for example no clear G2 cell cycle phase has been observed during schizogony (Arnot and Gull, 1998; Doerig et al., 2000). Furthermore, this asexual proliferation mode is characterised by multiple rounds of asynchronous nuclear division without chromosome condensation and in the absence of cytokinesis. Mitosis is closed, occurring without dissolution and reformation of the nuclear envelope, and the spindle-pole body (SPB)/microtubule-organising centre (MTOC), also known as the centriolar plaque (Arnot et al., 2011; Francia et al., 2015; Sinden, 1991a), is embedded within the nuclear membrane. The asynchronous nuclear division precedes cell division, leading to a multinucleate syncytium. The last round of nuclear division in these cells is synchronous and it is only after this final round of mitosis that cytokinesis occurs to form the haploid daughter merozoites or sporozoites, respectively.

The second type of mitotic division occurs during male gametogenesis (**Fig. 1 (B)**), following activation in the mosquito midgut. Three rounds of rapid genome duplication (from haploid to octoploid), without concomitant nuclear division (endoreduplication), are followed by chromosome condensation and nuclear budding into the flagellated male gamete during exflagellation within 12 to 15 min after activation (Arnot and Gull, 1998; Janse et al., 1988; Sinden, 1983). The resultant eight flagellated microgametes, each contain a haploid genome

(Guttery et al., 2015; Sinden et al., 2010). Fertilization of the haploid female gamete results in a diploid zygote, which develops and differentiates over a 24-hour period into a motile ookinete in the mosquito gut (**Fig. 1 (C)**). It is in this stage that meiosis occurs. The DNA is duplicated once to form a tetraploid cell and then two rounds of chromosome segregation result in four discrete haploid genomes prior to ookinete maturity while the nucleus remains intact without any division.. Reductive division to haploidy presumably occurs in the subsequent oocyst during sporozoite formation (Guttery et al., 2015; Sinden, 1991a; Sinden, 1991b). These different stages of cell division and proliferation indicate that the parasite has evolved alternate modes of chromosome replication, condensation and segregation, as well as nuclear and cell division at different stages during its life cycle.

The process of chromosome segregation and kinetochore dynamics which is the key role of the mitotic apparatus throughout the life cycle, is not well understood in *Plasmodium*. To date, analysis of *Plasmodium* mitotic/meiotic spindle assembly and chromosome segregation has been performed largely using transmission electron microscopy (TEM) (Sinden et al., 1978; Sinden et al., 1976), and biochemical analysis of microtubule markers including α-tubulin (Fennell et al., 2008), and centrins associated with the putative MTOC (Gerald et al., 2011; Roques et al., 2019). An analysis of a *Plasmodium* artificial chromosome (PAC) identified a putative centrosome derived from chromosome 5 (*PbCEN5*), and highlighted the dynamics of chromosome segregation during both mitotic and meiotic stages of the parasite's life cycle (Iwanaga et al., 2010). However, there is no real-time analysis of chromosome segregation dynamics during various proliferative stages, especially during stages that occur inside the mosquito vector. Here we have analysed the real-time expression and spatiotemporal dynamics of NDC80, as a kinetochore marker. We generated a stable transgenic *P. berghei* line expressing NDC80 with a C-terminal GFP-tag by modifying the endogenous locus. Using this tool, we examined NDC80 location with respect to spatiotemporal organisation of outer kinetochores during mitosis in schizogony, sporogony and male gametogenesis, and during meiosis in ookinete development. We observed unusual dynamics of kinetochores as clustered patterns of foci adjacent to the nuclear DNA during endomitotic nuclear division in asexual stages, with the number of foci corresponding to the likely ploidy of individual nuclei. However, kinetochores formed an unusual bridge-like pattern during endoreduplication stages in male gametogenesis. We show full complement of the NDC80 complex, with very a divergent, previously undetected, SPC24 component as determined by bioinformatics analysis. Altogether, we confirmed that this transgenic parasite line expressing NDC80 is a valuable resource for studying chromosome segregation and dynamics, as well as identifying the various protein complexes involved in these processes during cell division.

Results

To study kinetochore dynamics, we generated NDC80-GFP, a transgenic *P. berghei* line expressing NDC80 with a C-terminal GFP tag, by inserting the *gfp* coding sequence at the 3' end of the endogenous *Ndc80* locus using single homologous recombination (**Fig. S1A**). To complement our GFP-based imaging studies, we also generated a NDC80-mCherry line using the same strategy (**Fig. S1A**). Successful insertion was confirmed by PCR (**Fig. S1B**). Western blot analysis of a schizont protein extract using an anti-GFP antibody revealed the NDC80-GFP protein at the expected size of 96 kDa compared to the size of GFP alone at 29 kDa (**Fig. S1C**).

Following successful generation of the NDC80-GFP transgenic line, the spatiotemporal profile of NDC80-GFP protein expression and location was examined during the parasite life cycle at the three asexual mitotic replicative stages (liver and blood schizogony in the vertebrate host and oocyst development (sporogony) in the mosquito vector (**Fig. 1A**), the sexual mitotic stage (male gametogenesis) (**Fig. 1B**) and the meiotic stage (ookinete development) (**Fig. 1C**).

Real-time live cell imaging using NDC80-GFP reveals kinetochores aggregate as discrete foci during schizogony

In the asexual blood stage, no NDC80-GFP fluorescence was observed in the intra-erythrocytic ring stage, a non-replicative G1 phase of the cell cycle (Arnot and Gull, 1998; Arnot et al., 2011; Doerig et al., 2000) (**Fig. 2A**). A faint but discrete single focus of NDC80-GFP adjacent to the nuclear DNA was observed in the early trophozoite, which became more intense as the trophozoite developed (**Fig. 2A**). The late trophozoite stage marks the transition into early S phase of the cell cycle, when DNA synthesis starts; Onset of schizogony is the start of nuclear division and was marked by duplication of the NDC80-GFP signal into two foci lying in close proximity to each copy of nuclear DNA (stained using Hoechst), revealing that DNA replication and sister chromatid separation had occurred, as marked by the two kinetochore foci and followed by nuclear division. Similar fluorescence patterns were also observed in the NDC80-mCherry line (**Fig. S2**). We also observed asynchronous nuclear division during early schizogony, as marked by two or more nuclei with both single and double distinct NDC80 foci adjacent to single DNA masses (**Fig. 2A**). As alternating repeated S/M phases following the division of individual nuclei continued, these NDC80-GFP foci were duplicated several times into multiple foci. Further in-depth analysis of NDC80-GFP localization by super resolution microscopy confirmed the asynchronicity of nuclear division during blood stage schizogony (see **Fig. 2B and Supplementary video SV1, SV2 and SV 3**). This stage of DNA replication and nuclear

division is terminated by cytokinesis that only occurs at the end of the nuclear division phase (Arnot and Gull, 1998; Doerig et al., 2000). The short-lived, extracellular merozoite represents part of the G1 phase of the cell cycle (Arnot and Gull, 1998; Doerig et al., 2000). During schizogony in the pre-erythrocytic asexual stage in the liver, discrete fluorescent foci next to nuclear DNA were observed, which is similar to the pattern observed in blood stage schizogony (**Fig. S3**).

To complement the live-imaging analysis, erythrocytic schizogony was examined in ultrastructural studies. In the multinucleated schizont during merozoite formation, it was possible to identify nuclear/spindle poles directly adjacent to nuclear envelope with radiating microtubules and attached kinetochores on the inside of the nucleus **(Fig. 2C)**. However, these structures were not visible in the mature merozoite or the early intracellular ring stage. These observations are consistent with the live-imaging data.

Immunofluorescence imaging shows the arrangement of NDC80 (kinetochore) with centrin (putative MTOC/SPB) and spindles (α-tubulin)

To determine the relative position of NDC80-GFP with other mitotic markers, especially at the spindle and/or putative MTOC /SPB, we used immunofluorescence-based co-localization assays with anti-GFP antibodies, and anti-α-tubulin and anti-centrin, as markers for the spindle and putative MTOC/SPB, respectively. We observed that NDC80-GFP is located adjacent to alpha-tubulin that showed overlap between the NDC80 and alpha-tubulin signals in most of early schizonts (Sch-E) but not in late schizonts (Sch-L)(**Fig. 2D).** Similarly, using anti-GFP with anti-centrin antibodies, revealed that NDC80-GFP is located in close proximity to, but does not co-localize with centrin (**Fig. 2E**)

Rapid spindle dynamics of NDC80-GFP shows unusual kinetochore bridges during endo-reduplication in male gametogenesis

Given the remarkable speed and organisation of nuclear replication and chromosome segregation during male gametogenesis, we investigated the live cell dynamics of NDC80-GFP throughout this 15 min process following gamete activation *in vitro*. The results are presented in (**Fig. 3A)** including time-lapse screenshots (**Fig. 3B and C, Supplementary videos SV4 and SV5.**). In non-activated male gametocytes a single diffuse and faint NDC80-GFP focus was present (Fig S4A), which intensified to a sharp single focal point 1 minute post-activation (mpa) (**Fig. 3A**). By 2 mpa, this focal point extended to form a bridge across one side of the nucleus, followed by the separation of the two halves of the bridge to produce first two shorter linear rods that then contract to two clear single foci by 3 mpa (**Fig. 3A-C)**. A schematic diagram for this process (1-3 mpa) is shown in (**Fig 3D).** This unusual

linear arrangement of NDC80 shows the distribution of kinetochore elongates to approximately the full length of the nucleus, often arched around the nuclear margin, and maintains a consistent thickness of NDC80 suggesting that kinetochores are evenly spaced along this single linear element. This is different to metaphase in canonical systems, in which KTs form a metaphase plate perpendicular to the spindle axis. This process repeated twice, although non-synchronously, resulting in 8 discrete NDC80-GFP foci (**Fig. 3A**). To study the association of NDC80 with spindle the Indirect immunofluorescence assays were performed we used immunofluorescence-based co-localization assays with anti-GFP antibodies, and anti-α-tubulin. This showed clear co-localisation of NDC80 with microtubule marker both on the bridge like structure and the foci for NDC80 (**Fig.3E**)

The ultrastructural analysis of the nucleus during male gametogenesis within 8 mpa showed typical nuclear spindles with microtubules radiating from the nuclear poles, to which attached kinetochores could be identified dispersed along the length of the spindle (**Fig. 3F**). The spindles with attached kinetochores were located on the inner side of the nuclear membrane, (**Fig. 3F**). TEM images show that these kinetochores are dispersed along the length of the mitotic spindle from one spindle pole to the other (similar to the bridge observed in the fluorescence microscopy). This appears to be in contrast to a metaphase plate arrangement where kinetochores occur clusters at the midpoint of the spindle.

Following exflagellation, the eight discrete foci associated with endoreduplication disappeared rapidly and no NDC-GFP fluorescence was observed in flagellated motile microgametes (**Fig. S4A**). Furthermore, no NDC80-GFP fluorescence was observed in either non-activated or activated female gametocytes (**Fig. S4A**). To independently test for an association of NDC80 with microtubules, we tested for effects of anti-tubulin inhibitor (taxol) during male gametogenesis on NDC80 organisation. Addition of taxol at 1 min post activation blocked the progression of dynamic distribution of NDC80 in more than 80% of male gametocytes while DMSO treated gametocytes showed normal mitotic progression and NDC80 distribution **(Fig S4B).** This shows that NDC80 distribution and localization depend on spindle dynamics and can be blocked by taxol treatment, which affect microtubule cytoskeleton against depolymerisation. . To further, investigate the location of NDC80 in relation to the position of the centromere, NDC80-mCherry and the centromere-localised condensin core subunit SMC4-GFP line were crossed and used for live cell imaging of both markers to establish their spatiotemporal relationship as shown previously (Pandey et al., 2019). The location of both NDC80 and SMC4 was next to nucleus, showing co-localization **(Fig S4C)**. Similarly, the basal body/axoneme marker, Kinesin-8B-mCherry (Zeeshan et al., 2019a) crossed with NDC80-GFP line and showed that NDC80 is located away from the

basal body (kinesin-8B) during the start of male gametogenesis and later when kinesin-8B arranges across the axonemes (**Fig S4D).** To confirm the centromere-associated localisation of NDC80 in a genome-wide manner, we performed ChIP-seq experiment in activated gametocytes **(Fig S4E).** We observed strong ChiP-seq peaks at the centromeres of all 14 chromosomes similar to what was shown previously (Pandey et al., 2019).

NDC80-GFP shows unusual dynamics throughout the meiotic stages during zygote to ookinete differentiation.

Meiosis in the malaria parasite occurs during zygote differentiation to ookinete. This process takes 24 h to complete and during this time the ploidy of the parasite increases from 2N to 4N. To examine the behaviour of kinetochores throughout this process, we investigated the spatiotemporal profile of NDC80-GFP during ookinete differentiation.

NDC80-GFP fluorescence was first observed 1 to 1.5 h post-fertilization, as a single faint but distinct focal point, which gradually increased in intensity over the period 2 to 3 h post-fertilization (**Fig. 4**). Similar to male gametogenesis though no nuclear division is observed while the NDC80-GFP focus enlarged to form a pair of elongated rod-like features, with multiple foci evident during stages II to IV of ookinete development, ultimately resolving as 4 discrete foci in the mature ookinete 18 h post-fertilization which then has 4N genome (**Fig.4A**). The ultrastructure of the mature ookinete clearly showed four kinetochores clusters representing a 4N, but already segregated, genome within an intact nuclear membrane, consistent with the live cell imaging (**Fig. 4B**).

NDC80-GFP is present as multiple foci during oocyst development and sporozoite formation

During oocyst development and sporozoite formation, live cell imaging revealed NDC80-GFP fluorescence at multiple foci adjacent to the nuclear DNA during various stages of oocyst development from 7 days post-infection (dpi) of the mosquito to 21 dpi, as well as a single focus in mature sporozoites (**Fig. 5A and B**). Ultrastructure analysis of oocyst development revealed an enlarged nucleus that formed a large multiple lobed structure with multiple nuclear poles/centriolar plaques/ SPB / putative MTOC, followed by the formation of large numbers of sporozoites at the plasmalemma of the oocyst (**Fig. 5Bi**), as described previously (Ferguson et al., 2014; Schrevel et al., 1977). Detailed examination showed nuclear poles/centriolar plaques with kinetochores directed toward the developing sporozoites (**Fig. 5Bii**). The endomitotic process of sporozoite formation during sporogony resembles that of merozoite formation within host red cells and hence is similar to schizogony but with many more nuclei.

Immunoprecipitation of NDC80-GFP reveals all canonical members of the NDC80 complex, including a highly divergent SPC24 orthologue

Previous comparative genomics studies revealed evidence for the presence of three Ndc80 complex members in *Plasmodiidae*: NDC80, NUF2, SPC25, but did not find any candidate ortholog for SPC24 (van Hooff et al., 2017). In another apicomplexan lineage (*Cryptosporidium*) however, an SPC24 ortholog could be identified, raising the question whether SPC24 was truly lost in *Plasmodiidae* or whether a yet unidentified highly divergent ortholog could be present. To determine whether the composition of the NDC80 complex in *P. berghei* was truly divergent, including novel NDC80 interactors that might explain the distinct kinetochore localisations in different life stages, we performed immunoprecipitations against NDC80-GFP in 8 hour schizont cultures and gametocytes, 1 minute after activation. Mass spectrometric analysis of these pulldowns indeed recovered NUF2 (PBANKA_0414300) and SPC25 (PBANKA_1358800), but also four potential novel interactors (**Fig. 6B, Supplementary Table 3**): (1) PBANKA_1210200 is a clear ortholog of PRE-binding protein involved in transcription (Komaki-Yasuda et al., 2013). (2) PBANKA_1116800 is an ortholog of Brefeldin-A resistance protein, which is surprisingly absent in a number of eukaryotes (e.g. human and plants) and was shown to provide a link between the spindle pole body and the translation machinery in the budding yeast *Saccharomyces cerevisiae (Sezen et al., 2009)* . (3) PBANKA_1458300 is a kinesin of kinesin-13 family, which are motors involved in microtubule depolymerisation and potentially plays a role in spindle microtubule dynamics (Zeeshan et al., 2019b), and (4) PBANKA_1442300, a long coiled-coil protein with a predicted C-terminal globular domain that presented itself as a putative SPC24 ortholog. We could however not find any homologs outside of hematozoan lineages using conventional homology detection approaches, making the SPC24 inference problematic. We therefore constructed a large sequence database consisting of 64 apicomplexan and other eukaryotic genomes and transcriptomes (**Supplementary Table 2**), and compared Hidden Markov Models (HMM) of automatically defined homologous groups of sequences with HMM profiles of PBANKA_1442300-like homologs and bona fide eukaryotic SPC24 orthologs found in our dataset (see methods). This approach yielded additional SPC24 orthologs in a multi-step manner (**Fig. 6C**): hematozoan homologs (including PBANKA_1442300) were significantly similar ($E > 10^{-5}$) to the previously unannotated group of coccidian homologous sequences (including the *Toxoplasma gondii* gene TGME49_212800). The merged HMM profile of these two groups, in turn, was significantly similar to that of eukaryote-wide SPC24 orthologs ($E > 10^{-5}$),

meaning that both PBANK_1442300 and TGME49_212800 can be classified as bona fide SPC24 orthologs (**Supplementary Sequence File 1, Supplementary Table 3**).

Discussion

Cellular proliferation in eukaryotes requires chromosome replication and precise segregation, followed by cell division, to ensure that daughter cells have identical copies of the genome. This happens through assembly of a spindle to which the centromeric region of chromosomes are attached through the kinetochore. Although the organisation of spindle microtubules, the molecular composition of kinetochores, and the modes of spindle pole separation vary extensively among eukaryotes (Akiyoshi and Gull, 2013; Drechsler and McAinsh, 2012; van Hooff et al., 2017), the microtubule-binding subunit NDC80 is conserved across most eukaryotes, including apicomplexan parasites such as *Toxoplasma gondii* and *Plasmodium spp.* (Akiyoshi and Gull, 2013; Farrell and Gubbels, 2014; van Hooff et al., 2017). In addition, since chromosomes only bare one kinetochore, the outer-kinetochore subunit NDC80 presents itself as a good tool to start probing the rather surprising chromosome dynamics during the different stages of the life cycle in *P. berghei*.

In this study we have sought to understand the assembly and dynamics of the mitotic machinery in the diverse modes of nuclear division in *Plasmodium* using the kinetochore-protein NDC80 as a marker for chromosome attachment to the mitotic spindle. For this we generated a transgenic parasite line to express endogenous C terminal GFP-labelled NDC80, a protein which faithfully replicates kinetochore location and function during all diver mitotic and meiotic stages stages of the life cycle. Live-cell imaging of the fluorescent protein, complemented with ultrastructural studies by electron microscopy, revealed a subcellular location of NDC80-GFP at discrete foci adjacent to nuclear DNA in all replicative stages of the *P. berghei* life cycle. The distribution and dynamic spatiotemporal profile corresponded to the replication of chromosomes during the atypical mitotic and meiotic processes of DNA replication in this organism. Non-replicating stages, including the intraerythrocytic ring stage, the extracellular mature merozoite, the non-activated female gametocyte and the motile male gametes show no evidence of kinetochore assembly as observed no Ndc80-GFP expression was observed. Using a combination of GPF-pulldown and a sensitive homology detection workflow we identified all four components of the NDC80 complex throughout apicomplexans, including in Plasmodiidae

The subcellular localization data for NDC80-GFP revealed a discreet single focus adjacent to the haploid nuclear genome, which presumably contains the centromeres of all 14

chromosomes. Such clustering of centromeric regions has been demonstrated in yeast (Richmond et al., 2013), human cells (Solovei et al., 2004) and *Toxoplasma* (Farrell and Gubbels, 2014). It is thought to be important for genome integrity, but the exact reason for it is not well understood. In the stages of the life cycle where this NDC80 clustering is not detected, perhaps the 14 kinetochores are not fully assembled and therefore NDC80-GFP expression is not detectable (Hoeijmakers et al., 2012). This is consistent with the idea that clustering of centromeres in *P. falciparum* occurs only prior to the onset of chromosome segregation (Hoeijmakers et al., 2012). It is of interest that following fertilization there is a single focus despite the genome being diploid, this may well reflect the tight pairing of sister chromatids allowing recombination to occur at this stage.

Although our data showed a clustered location of NDC80, its actual role in chromosome clustering is not known. Previous studies on yeast and *Toxoplasma* showed no role of NDC80 in clustering, and suggested a sole role in attachment to spindle MTs during chromosome segregation. A single MT binds each kinetochore in budding yeast (Westermann et al., 2007); whereas in *Toxoplasma* a maximum of only 11 MTs were detected despite the fact that there are 13 chromosomes (Bunnik et al., 2019; Farrell and Gubbels, 2014; Swedlow et al., 2002). Within the closely related Coccidian parasites, a number of variations in the details of the process of asexual division have been described, relating to timing and number of genome and nuclear divisions (Ferguson et al., 2008) The coccidian parasite *Sarcocystis neurona*, which divides by endopolygeny forms a polyploid nucleus culminating in 64 haploid daughter cells (Farrell and Gubbels, 2014; Vaishnava et al., 2005). During this process, intranuclear spindle poles are retained throughout the cell cycle, which suggests constant attachment of chromosomes to spindle MTs to kinetochores to ensure genome integrity throughout *Sarcocystis* cell division (Farrell and Gubbels, 2014; Vaishnava et al., 2005). In contrast, *Plasmodium* (a hemosporidian), undergoes classical schizogony with a variable number of cycles of genome replication and nuclear division resulting a multinucleated cell (Arnot et al., 2011). This is similar to what is seen in the coccidian parasites *Eimeria* spp and *Toxoplasma,* with daughter cell formation being associated with the final nuclear division. This fact is well demonstrated by the NDC80 localization in this study, which shows 1 or 2 NDC80-GFP foci per nucleus. The asynchronous nature of the division during these stages is shown by nuclei having either one or two NDC80-GFP foci (and intermediate forms) within the same cell. We made similar observations in our previous study of the SPB/MTOC/ centriole plaque marker for centrin, CEN-4 (Roques et al., 2019). These studies also suggest that the kinetochore and centrosome/centriolar plaque body duplicate before nuclear division starts; therefore the duplication of NDC80 and CEN-4 sets the stage for mitosis at each round of nuclear division

in *Plasmodium,* as in *Toxoplasma* (Suvorova et al., 2015). In contrast, during male gametogenesis the genome size increases to 8N, and this corresponds to the formation of 8 distinct NDC80-GFP foci, before nuclear division, with asynchronous chromosome replication and segregation. Most notable is the presence of unique kinetochore bridges or rod-like structures during genome replication and chromosome segregation. It appears that two hemi-spindles associated with the kinetochores are joined together to form a mitotic spindle at the earliest stages of endo reduplications during male gametogenesis. This is then followed by kinetochore movement to opposite poles once all the duplicated chromosomes are segregated. The mitotic process of duplication proceeds in the absence of nuclear division (karyokinesis), which results in very atypical kinetochore dynamics but consistent with the live cell imaging data.

Similarly, during meiosis in ookinete development the genome size increases to 4N, represented by bridge-like kinetochore structures during replicative stages and at the end resulting in four distinct NDC80-GFP foci suggesting kinetochore clustering to facilitate chromosome segregation although no nuclear division takes place.

During sporogony multiple lobes are formed and the intranuclear spindle may be formed during multiple nuclear divisions as revealed by ultrastructural studies during sporozoite formation (Schrevel et al., 1977). Further ultrastructure analyses identified typical nuclear spindles with attached kinetochores, radiating from the nuclear poles located within an intact nuclear membrane during schizogony, male gametogenesis, ookinete development and sporogony. Our data are consistent with a previous report, in which kinetochore localization was revealed using ultrastructural studies of *P. berghei* sporogony, and the duplication of hemi-spindles during replication was suggested (Schrevel et al., 1977). Overall, based on all these results, consistent kinetochore clustering occurs within Apicomplexa.

NDC80 is a major constituent of kinetochores and is highly conserved among eukaryotes including *Plasmodium.* However, many of the molecular details of kinetochore architecture and function in *Plasmodium* remain to be explored. A recent comparative evolutionary analysis suggested a distinct kinetochore network in many eukaryotes including *P. falciparum* and other Alveolates, with many of the highly conserved kinetochore complex proteins being absent in Plasmodium (van Hooff et al., 2017). Of 70 conserved kinetochore proteins only eleven are encoded in the *P. falciparum* genome. These eleven proteins include NDC80, NUF2, CENP-C/-A/-E, SPC25 and others that are highly conserved across 90 eukaryotic species, but genes for many other conserved proteins like SPC24, MAD-1/-2) and MIS12 were found to be absent (van Hooff et al., 2017). Recent studies have shown the presence of unconventional kinetochore proteins in kinetoplastids (Akiyoshi and Gull, 2013;

D'Archivio and Wickstead, 2017), suggesting that different kinetochore architectures are possible. Previous reports have shown the association of CENP-A and CENP-C with centromeres in *P. falciparum* (Verma and Surolia, 2013; Verma and Surolia, 2014).. Using a combination of GPF-pulldown and a sensitive homology detection workflow we identified all components of the NDC80 complex throughout apicomplexans, including in Plasmodiidae. Previous studies in *Toxoplasma gondii* could only identify NDC80 and NUF2 (Farrell and Gubbels, 2014), but we here predicted the presence of SPC25 (TGME49_232400) and SPC24 (TGME49_212800). Our approach illustrates that conspicuous absences of subunits of highly conserved and essential complexes, such as the obligate tetrameric NDC80 complex are to be treated with caution, and additional sensitive homology searches using HMM-HMM comparison should be employed to more thoroughly test for homolog presences or absences. As such, patterns of loss have been observed in eukaryotic parasites before, and we expect that systematic searches for conspicuous absences of subunits of specific complexes, will yield a large number of highly divergent homologs in Apicomplexa.

NDC80 and NUF2, appear to be the most conserved subunits of the NDC80 complex, but the SPC24-SPC25 dimer that interacts with the centromere is highly divergent, both in sequence and in length. The average length of SPC24 orthologs in Plasmodiidae and Sarcocystidae for instance are 3-4 times longer than those of other eukaryotes. What this means exactly is unclear, but we speculate that the NDC80 complex in Apicomplexa engages centromere-proximal kinetochore proteins, such as CENP-A and CENP-C in a different manner to other eukaryotes. Although, this is supported by the absence of the canonical interaction partners of SPC24 and SPC25, namely CENP-T and the MIS12 complex (van Hooff et al., 2017), the extended length of SPC24 is not seen in all Apicomplexa, and therefore different lineages may have different ways of incorporating the Ndc80 complex into the kinetochore. The extended length of *Plasmodium* and coccidian (e.g. in *T. gondii*) SPC24 could potentially provide additional binding sites for novel interactors that may drive either kinetochore clustering and/or the remarkable ‘bridge/rod’ phenotype we have observed in this study. Our NDC80-GPF pulldown identified three other potential interactors. Of these, the ortholog of Brefeldin-A resistance protein (Bfr1; PBANKA_1116800) is the most intriguing candidate as it was found to provide a link between the spindle pole body and the translation machinery in the budding yeast *Saccharomyces cerevisiae* (Sezen et al., 2009). Whether this protein plays a role in the kinetochore is unclear, and future localisation studies and knockdown experiments will have to show its potential role in the kinetochore and chromosome segregation.

In summary, this study demonstrates the dynamic expression and location of NDC80 during the different proliferative stages of the malaria parasite and reveals both the disassembly

and reassembly and clustering of kinetochores. It also shows the asynchronous closed mitotic division of *Plasmodium* during schizogony and sporogony, and provides novel insights into the chromosome segregation in male gametogenesis and in various stages of meiosis during zygote differentiation to ookinetes. Chip seq and colocalisation studies clearly showed the centromeric location of NDC80 in *Plasmodium*. The protein pulldown and bioinformatics studies revealed that NDC80 has the full complement of four subunits, though SPC24 is highly divergent compared to other eukaryotes. This analysis of NDC80 will facilitate future studies of cell division and comparative analyses of chromosome dynamics in evolutionary divergent eukaryotic cells

Material and Methods:

Ethical statement

All animal-related work performed at the University of Nottingham has undergone an ethical review process and been approved by the United Kingdom Home Office with the project license number 30/3248 and PDD2D5182. The work has been carried out in accordance with the United Kingdom 'Animals (Scientific Procedures) Act 1986' and was in compliance with 'European Directive 86/609/EEC' for the protection of animals used for experimental purposes. A combination of ketamine followed by antisedan was used for general anaesthesia and sodium pentobarbital was used for terminal anaesthesia. Proper care and efforts were made to minimise animal usage and suffering.

Six to eight-week-old female Tuck-Ordinary (TO) (Harlan) or CD1 outbred mice (Charles River) were used for all experiments.

Generation of transgenic parasites

The transgenic lines for NDC80 (PBANKA_1115700) were created using single homologous recombination as shown in **Fig. S1**. The oligonucleotides used to generate transgenic lines are provided in **Supplementary Table S1**. For GFP tagging, a 1153bp region of *Ndc80* without the stop codon was inserted upstream of the *gfp* sequence in the p277 plasmid vector using KpnI and ApaI restriction sites as described previously (Tewari et al., 2010). The p277 vector contains the human *dhfr* cassette, conveying resistance to pyrimethamine. Before transfection, the sequence was linearised using EcoRV. The *P. berghei* ANKA line 2.34 was used for transfection by electroporation (Janse et al., 2006). Immediately, electroporated parasites were mixed with 100µl of reticulocyte-rich blood from a phenylhydrazine (6 mg/ml, Sigma) treated, naïve mouse and incubated at 37°C for 30 min before intraperitoneal injection. Pyrimethamine (70 mg/L, Sigma) was supplied in the drinking water from 1-day post-infection (dpi) to 4-dpi. Infected mice were monitored for 15 days and drug selection was repeated after passage to a second mouse. Integration PCR and western blot were performed to confirm successful generation of the transgenic line. For integration PCR, primer 1 (IntT259) and primer 2 (ol492) were used to confirm integration of the GFP targeting construct. Primer 1 and primer 3 (T2592) were used as a control. We also generated a mCherry-tagged NDC80 transgenic parasite line as shown in the schematic provided in **Fig. S1.**

Western Blot

For western blotting, purified schizonts were lysed using lysis buffer (10 mM TrisHCl pH 7.5, 150 mM NaCl, 0.5 mM EDTA, 1% NP-40 and 1% Sarkosyl). The samples were boiled for 10 min after adding Laemmli sample buffer to the lysed cells. The sample was centrifuged at 13500 g for 5 min and electrophoresed on a 4–12% SDS-polyacrylamide gel. Subsequently, resolved proteins were transferred to nitrocellulose membrane (Amersham Biosciences) and immunoblotting was performed using the Western Breeze Chemiluminescence Anti-Rabbit kit (Invitrogen) and anti-GFP polyclonal antibody (Invitrogen) at a dilution of 1:1250, according to the manufacturer's instructions.

Localization of NDC80-GFP throughout the parasite life cycle

Live cell imaging of transgenic parasite lines was performed at different proliferative stages during the parasite life cycle (Figure 1) as described previously (Roques et al., 2019; Saini et al., 2017) using a Zeiss AxioImager M2 microscope fitted with an AxioCam ICc1 digital camera (Carl Zeiss, Inc).

Blood stage schizogony

Infected mouse blood provided asexual blood and gametocyte stages of the *P. berghei* life cycle. Schizont culture (RPMI 1640 containing 25 mM HEPES, 1:10 (v/v) fetal bovine serum and penicillin/streptomycin 1:100) at different time points was used to analyse various stages of asexual development from ring to merozoite. The periods used for analysis and imaging werer 0 to1 h for ring stage parasites, 2 to 4 h for trophozoites, 6 to 8 h for early and mid-stage schizonts, 9 to 11 h for late segmented schizonts, and 18 to 24 h for mature schizonts and released merozoites in schizont culture medium.

Male gametocyte development

In vitro cultures were prepared to analyse non-activated gametocytes, activated gametocytes and male exflagellation. For *in vitro* exflagellation studies, gametocyte-infected blood was obtained from the tails of infected mice using a heparinised pipette tip. Gametocyte activation was performed by mixing 100µl of ookinete culture medium (RPMI 1640 containing 25 mM HEPES, 20% fetal bovine serum, 10 mM sodium bicarbonate, 50 µM xanthurenic acid at pH 7.6) with gametocyte-infected blood. To study different time points during microgametogenesis, gametocytes were purified using Nycodenz gradient (48%) and monitored at different time points to study mitotic division (male gametogenesis, 0 to 15 min post-activation (mpa).

Ookinete development

To study ookinete development, gametocyte infected blood was incubated in ookinete medium for 24 hpa and various stages of zygote differentiation and ookinete development were monitored at different time points (0 min for nonactivated gametocytes, 30 min for activated gametocytes, 2 to 3 h for zygotes, 4 to 5 h for stage I, 5 to 6 h for stage II, 7 to 8 h for stage III, 8 to 10 h for stage IV, 11 to 14h for stage V, and 18 to 24 h for mature ookinetes post activation in ookinete medium).

Oocyst and sporozoite development

For mosquito transmission stages and bite back experiments, triplicate sets of 30 to 50 *Anopheles stephensi* mosquitoes were used. The mosquito guts were analysed on different days post-infection (dpi): 7 dpi, 12 dpi, 14 dpi and 21 dpi to check expression and localization of NDC80GFP during oocyst development and sporozoite formation.

Schizogony in liver stages

To study localization of NDC80-GFP in *P. berghei* liver stages, 100,000 HeLa cells were seeded in glass-bottomed imaging dishes. Salivary glands of female *A. stephensi* mosquitoes infected with NDC80-GFP parasites were isolated and sporozoites were released using a pestle to disrupt salivary gland cells. The released sporozoites were pipetted gently onto the HeLa cells and incubated at 37 °C in 5% CO_2 in air, in complete minimum Eagle's medium containing 2.5 µg/ml amphotericin B. For initial infection, medium was changed at 3 h post-infection and thereafter once a day. To perform live cell imaging, Hoechst 33342 (Molecular Probes) was added (1 µg/ml) and imaging was done at 55 h post-infection using a Leica TCS SP8 confocal microscope with the HC PL APO 63x/1.40 oil objective and the Leica Application Suite X software.

Indirect immunofluorescence assay

IFA studies were performed using poly-L-lysine coated slides on which schizonts had been previously fixed in 2% paraformaldehyde (PFA) in microtubule stabilising buffer (MTSB:10 mM MES, 150 mM NaCl, 5 mM EGTA, 5 mM $MgCl_2$, 5 mM glucose) in 1X-PBS for 30 min at room temperature (RT) and smeared onto slides. The fixed cells were permeabilized using TBS containing 0.2% TritonX-100 for 5 min and washed three times with TBS before blocking. For blocking, 1hour incubation was performed with TBS solution containing 3% BSA (w/v) and 10% goat serum (v/v). TBS containing 1% BSA and 1% goat serum was used to dilute the antibodies for the incubations. Anti-GFP rabbit antibody (Invitrogen) was used at 1:250 dilution, anti-alpha-tubulin mouse antibody (Sigma-Aldrich) was used at 1:1000 dilution, and anti-centrin mouse clone 20h5 antibody (Millipore) was used at 1:200 dilution;

each was incubated for 1 hour at RT. Three washes were performed with TBS, then AlexaFluor 568 labelled anti-rabbit (red) and AlexaFluor 488 labelled anti-mouse (green) (Invitrogen) (1:1000 dilution) were used as secondary antibodies and incubated for 40 min at RT. A similar protocol was followed for gametocytes except the cells were fixed in 4% PFA in MTSB. Slides were mounted with Vectashield containing DAPI (blue) and sealed using nail polish. Images were captured as described for live imaging.

Super resolution microscopy

A small volume (3 µl) of schizont culture was mixed with Hoechst dye and pipetted onto 2 % agarose pads (5x5 mm squares) at room temperature. After 3 min these agarose pads were placed onto glass bottom dishes with the cells facing towards glass surface (MatTek, P35G-1.5-20-C). Cells were scanned with an inverted microscope using Zeiss C-Apochromat 63×/1.2 W Korr M27 water immersion objective on a Zeiss Elyra PS.1 microscope, using the structured illumination microscopy (SIM) technique. The correction collar of the objective was set to 0.17 for optimum contrast. The following settings were used in SIM mode: lasers, 405 nm: 20%, 488 nm: 50%; exposure times 100 ms (Hoechst) and 25 ms (GFP); three grid rotations, five phases. The band pass filters BP 420-480 + LP 750 and BP 495-550 + LP 750 were used for the blue and green channels, respectively. Multiple focal planes (Z stacks) were recorded with 0.2 µm step size; later post-processing, a Z correction was done digitally on the 3D rendered images to reduce the effect of spherical aberration (reducing the elongated view in Z; a process previously tested with fluorescent beads). Images were processed and all focal planes were digitally merged into a single plane (Maximum intensity projection). The images recorded in multiple focal planes (Z-stack) were 3D rendered into virtual models and exported as images and movies (see supplementary material). Processing and export of images and videos were done by Zeiss Zen 2012 Black edition, Service Pack 5 and Zeiss Zen 2.1 Blue edition.

Chromatin Immuno Precipitation Sequencing analysis

For the ChIP-seq analysis, libraries were prepared from crosslinked cells (using 1% formaldehyde). The crosslinked parasite pellets were resuspended in 1 mL of nuclear extraction buffer (10 mM HEPES, 10 mM KCl, 0.1 mM EDTA, 0.1 mM EGTA, 1 mM DTT, 0.5 mM AEBSF, 1X protease inhibitor tablet), post 30 min incubation on ice, 0.25% Igepal-CA-630 was added and homogenized by passing through a 26G x ½ needle. The nuclear pellet extracted through 5000 rpm centrifugation, was resuspended in 130 µl of shearing buffer (0.1% SDS, 1 mM EDTA, 10 mM Tris-HCl pH 7.5, 1X protease inhibitor tablet), and transferred to a 130 µl Covaris sonication microtube. The sample was then sonicated using

a Covaris S220 Ultrasonicator for 10 min for schizont samples and 6 min for gametocyte samples (Duty cycle: 5%, Intensity peak power: 140, Cycles per burst: 200, Bath temperature: 6°C). The sample was transferred to ChIP dilution buffer (30 mM Tris-HCl pH 8, 3 mM EDTA, 0.1% SDS, 30 mM NaCl, 1.8% Triton X-100, 1X protease inhibitor tablet, 1X phosphatase inhibitor tablet) and centrifuged for 10 min at 13,000 rpm at 4°C, retaining the supernatant. For each sample, 13 µl of protein A agarose/salmon sperm DNA beads were washed three times with 500 µl ChIP dilution buffer (without inhibitors) by centrifuging for 1 min at 1000 rpm at room temperature, then buffer was removed. For pre-clearing, the diluted chromatin samples were added to the beads and incubated for 1 hour at 4°C with rotation, then pelleted by centrifugation for 1 min at 1000 rpm. Supernatant was removed into a LoBind tube carefully so as not to remove any beads and 2 µg of anti-GFP antibody (ab290, anti-rabbit) were added to the sample and incubated overnight at 4°C with rotation. Per sample, 25 µl of protein A agarose/salmon sperm DNA beads were washed with ChIP dilution buffer (no inhibitors), blocked with 1 mg/mL BSA for 1 hour at 4°C, then washed three more times with buffer. 25 µl of washed and blocked beads were added to the sample and incubated for 1 hour at 4°C with continuous mixing to collect the antibody/protein complex. Beads were pelleted by centrifugation for 1 min at 1000 rpm at 4°C. The bead/antibody/protein complex was then washed with rotation using 1 mL of each buffers twice; low salt immune complex wash buffer (1% SDS, 1% Triton X-100, 2 mM EDTA, 20 mM Tris-HCl pH 8, 150 mM NaCl), high salt immune complex wash buffer (1% SDS, 1% Triton X-100, 2 mM EDTA, 20 mM Tris-HCl pH 8, 500 mM NaCl), high salt immune complex wash buffer (1% SDS, 1% Triton X-100, 2 mM EDTA, 20 mM Tris-HCl pH 8, 500 mM NaCl), TE wash buffer (10 mM Tris-HCl pH 8, 1 mM EDTA) and eluted from antibody by adding 250 µl of freshly prepared elution buffer (1% SDS, 0.1 M sodium bicarbonate). We added 5 M NaCl to the elution and cross-linking was reversed by heating at 45°C overnight followed by addition of 15 µl of 20 mg/mL RNAase A with 30 min incubation at 37°C. After this, 10 µl 0.5 M EDTA, 20 µl 1 M Tris-HCl pH 7.5, and 2 µl 20 mg/mL proteinase K were added to the elution and incubated for 2 hours at 45°C. DNA was recovered by phenol/chloroform extraction and ethanol precipitation, using a phenol/chloroform/isoamyl alcohol (25:24:1) mixture twice and chloroform once, then adding 1/10 volume of 3 M sodium acetate pH 5.2, 2 volumes of 100% ethanol, and 1/1000 volume of 20 mg/mL glycogen. Precipitation was allowed to occur overnight at -20°C. Samples were centrifuged at 13,000 rpm for 30 min at 4°C, then washed with fresh 80% ethanol, and centrifuged again for 15 min with the same settings. Pellet was air-dried and resuspended in 50 µl nuclease-free water. DNA was purified using Agencourt AMPure XP beads. Libraries were prepared using the KAPA Library Preparation Kit (KAPA Biosystems), and were amplified for a total of 12 PCR cycles (15 s at 98°C, 30 s at 55°C, 30 s at 62°C) using the KAPA HiFi HotStart Ready Mix (KAPA

Biosystems). Libraries were sequenced using the NovaSeq 6000 System (Illumina), producing 100-bp reads.

FastQC (https://www.bioinformatics.babraham.ac.uk/projects/fastqc/), was used to analyze raw read quality. Any adapter sequences were removed using Trimmomatic (http://www.usadellab.org/cms/?page=trimmomatic). Bases with Phred quality scores below 25 were trimmed using Sickle (https://github.com/najoshi/sickle). The resulting reads were mapped against the *P. berghei* ANKA genome (v36) using Bowtie2 (version 2.3.4.1) or HISAT2 (version 2-2.1.0), using default parameters. Reads with a mapping quality score of 10 or higher were retained using Samtools (http://samtools.sourceforge.net/), and PCR duplicates were removed by PicardTools MarkDuplicates (Broad Institute). For Chip-seq analysis, raw read counts were determined to obtain the read coverage per nucleotide. Genome browser tracks were generated and viewed using the Integrative Genomic Viewer (IGV) (Broad Institute). Proposed centromeric locations were obtained from Iwanaga and colleagues (Iwanaga et al., 2010).

Inhibitor studies

Gametocytes were purified as above and treated with taxol (1µm) (Paclitaxel, T7402; Sigma) at 1 min post activation (mpa) and then fixed with 4% Paraformaldehyde (PFA) at 8 mpa. DMSO was used as a control treatment. These fixed gametocytes were then examined on a Zeiss Axio Imager M2 microscope fitted with an AxioCam ICc1 digital camera (Carl Zeiss, Inc).

Electron microscopy

Samples for different mitotic stages of parasite development including schizonts (24 hours in culture), activated male gametocytes (8 min post-activation), infected mosquito guts (12 to 14 days post infection) and the meiotic stage from the mature ookinete (24hours post-activation) were fixed in 4% glutaraldehyde in 0.1 M phosphate buffer and processed for electron microscopy as previously described (Ferguson et al., 2005). Briefly, samples were post-fixed in osmium tetroxide, treated in bloc with uranyl acetate, dehydrated and embedded in Spurr's epoxy resin. Thin sections were stained with uranyl acetate and lead citrate prior to examination in a JEOL1200EX electron microscope (Jeol UK Ltd).

Immunoprecipitation and Mass Spectrometry

Schizonts, following 8 hours *in vitro* culture, and male gametocytes 1 min post activation of NDC80-GFP parasites were used to prepare cell lysates. Purified parasite pellets were crosslinked using formaldehyde (10 min incubation with 1% formaldehyde in PBS),

followed by 5 min incubation in 0.125M glycine solution and 3 washes with phosphate buffered saline (PBS, pH 7.5). Immunoprecipitation was performed using crosslinked protein lysate and a GFP-Trap®_A Kit (Chromotek) following the manufacturer's instructions. Proteins bound to the GFP-Trap®_A beads were digested using trypsin and the peptides were analysed by LC-MS/MS. Mascot (http://www.matrixscience.com/) and MaxQuant (https://www.maxquant.org/) search engines were used for mass spectrometry data analysis. PlasmoDB database was used for protein annotation. Peptide and proteins having minimum threshold of 95% were used for further proteomic analysis. The mass spectrometry proteomics data have been deposited to the ProteomeXchange Consortium via the PRIDE partner repository with the dataset identifier PXD017619 and 10.6019/PXD017619.

Comparative genomics of the NDC80 complex in Apicomplexa

Database: To increase the sensitivity for detecting highly divergent members of the NDC80 complex (NDC80, NUF2, SPC25, SPC24) in apicomplexan parasites, we constructed a large sequence database of (new) genomes and (meta)transcriptomes (see **Supplementary Table 2** for sources). This database consisted of 43 apicomplexans and 8 Apicomplexa-affliated lineages, including newly sequenced gregarines and 'apicomonada' (Janouskovec et al., 2019; Janouskovec et al., 2015; Mathur et al., 2019), and the non-parasitic apicomplexan *Nephromyces* (Munoz-Gomez et al., 2019). A set of 13 eukaryotes representative of a wider range of the eukaryotic tree of life were added for which the NDC80 complex presence/absence pattern was studied previously (van Hooff et al., 2017) For transcriptomes for which no gene predictions were available, ORFs were predicted using TransDecoder (Long Orfs algorithm: https://github.com/TransDecoder/TransDecoder).

Ortholog detection***:*** To uncover an initial set of sequences orthologous to NDC80 complex subunits in our database we made use of previously established eukaryote-wide Hidden Markov Models (HMM) of the Calponin Homology domains of NDC80 and NUF2, and the RWD domains for SPC24 SPC25 (Tromer et al., 2019; van Hooff et al., 2017). Although potentially informative, coiled-coil regions where avoided as they tend to have sequence similarities with (other) non-homologous coiled-coil proteins. For details on the strategy for finding orthologs, see previously established protocols (van Hooff et al., 2017). Briefly, HMM-guided hits were realigned using mafft (option:eins-i) (Katoh and Standley, 2013), modelled as HMM, and searched iteratively against the database until no new orthologs could be detected. Conspicuous absences were further inspected by iterative searches using sequences of closely-related lineages, including lower stringency matches (higher E-values, lower bitscores) that had a similar length and coiled-coil topology. HMMs were modelled

(hmmbuild) and iteratively searched (hmmsearch or jackhmmer: E-value<0.05, bitscore>25) using the HMMER package (v3.1b) *(Johnson et al., 2010).* SPC24 orthologues in Coccidia and Hematozoa were detected by comparing our custom-made eukaryote-wide HMMs with HMM profiles of automatically defined orthologous groups (OrthoFinder (Emms and Kelly, 2019)), using the secondary structure aware HMM-vs-HMM search algorithm HHsearch (Steinegger et al., 2019). Specifically, HMM profiles of the orthologous groups containing PBANKA_1442300 (*P. berghei*) and TGME49_212800 (*T. gondii)* were merged and the resulting HMM was searched against a dataset containing HMMs of the orthologous groups defined by OrthoFinder, a previously established set containing scop70, pdb70 and PfamA version 31.0 [7], and custom-made HMM of kinetochore proteins (Tromer et al., 2019; van Hooff et al., 2017).

Alignments were visualised and modified using Jalview (Waterhouse et al., 2009). Figure 6 was made using Inkscape (https://inkscape.org/).

Competing interests

The authors declare no competing interests.

Acknowledgements

We thank Prof. Snezhana Oliferenko, The Francis Crick Institute, for stimulating discussions and advice on kinetochore proteins.

Author contribution

RT conceived and designed all experiments. RT, MZ, ED and DB performed the experiments; RRS performed liver stage imaging; RP and RM performed super-resolution imaging; DJPF performed electron microscopy; ET and RW performed the bioinformatics and phylogenetic analysis; SA and KLR performed the ChIP-seq analysis; MZ, RT and ARB performed pulldown experiments, RP, MZ, AAH, and RT analysed the data; MZ, RP DSG, ET, RW AAH and RT wrote the manuscript and all others contributed to it.

Funding

This project was funded by MRC project grants and MRC Investigators grants awarded to RT (G0900109, G0900278, MR/K011782/1) and BBSRC grant to RT (BB/N017609/1). RP was supported on MRC project grant MR/K011782/1 and M Z is supported on BBSRC grant BB/N017609/1 to RT. AAH was supported by the Francis Crick Institute (FC001097), which receives its core funding from Cancer Research UK (FC001097), the UK Medical Research Council (FC001097), and the Wellcome Trust (FC001097). KGLR was supported by the

National Institutes of Allergy and Infectious Diseases and the National Institutes of Health (grants R01 AI06775 and R01 AI136511) and the University of California, Riverside (NIFA-Hatch-225935). ET is funded by a postdoctoral research fellowship of the Herchel Smith Fund from the University of Cambridge. The super resolution microscope facility was funded by the BBSRC grant BB/L013827/1.

Figure legends:

Fig. 1: Life cycle of rodent malaria parasite *Plasmodium berghei*. (**A)** represents endomitotic division: schizogony (schizont formation) in the liver and blood cells of the mammalian host and sporogony (sporozoite formation) in the mosquito gut. (**B)** and **(C)** represent atypical mitotic division by endoreduplication during male gametogenesis and meiotic division during the zygote to ookinete differentiation in the mosquito gut, respectively.

Fig. 2: NDC80-GFP localization during endomitotic cell division in schizogony. **(A)** Live cell imaging of NDC80-GFP expression and location during asexual blood stage (DIC: Differential interference contrast, Hoechst: DNA, NDC80-GFP: GFP, Merge: Hoechst and GFP fluorescence, Troph: Trophozoite, Sch-E: Early Schizont, Sch-M: Mid Schizont Sch-L: Late Schizont, Mero: Merozoite, 100x magnification, Scale bar = 5 µM.) and schematic guide depicting NDC80 localization during various developmental stages in the bloodstream of the parasite life cycle. **(B)** Live cell super-resolution 3D imaging for NDC80-GFP localization during asynchronous blood stage mitotic division. Scale bar = 5 µM. (**C)** Electron microscopy imaging of an early schizont showing kinetochore localization. **(i)** Section through an early schizont within a red blood cell, showing two nuclei (N) and the food vacuole (FV). Scale bar = 1 µm. **(ii)** Enlargement of the enclosed area showing part of the nucleus in which a nuclear pole (NP), microtubules and attached kinetochores (K) can be seen. Scale bar = 100 nm. (**D)** Immunofluorescence fixed cell imaging and schematic guide of NDC80-GFP and co-localization with α-tubulin showing overlap during early schizont (**E**) Immunofluorescence fixed cell imaging and schematic guide of NDC80-GFP and co-localization with centrin (100x magnification). Scale bar = 5 µM.

Fig. 3: Temporal dynamics of NDC80-GFP during male gametogenesis. (A) Live cell imaging for NDC80-GFP expression and location during endoreduplicative mitotic division in male gametogenesis (100x magnification) **(B-C)** Time-lapse screenshots for NDC80-GFP localization during male gametogenesis. Scale bar = 5 µM. (**D)** Schematic representation showing dynamic localization of NDC80 during 1-3 min post activation of gametocyte (first round of nuclear division). **(E)** Indirect immunofluorescence assays showing co-localization of NDC80 (red) and α-tubulin (green) in male gametocytes activated for 1-3 min. **(F)** Electron microscopy on 8 min post-activation gametocytes for kinetochore localization. **(i)** Section

through a mid-stage microgametocyte showing the large central nucleus (N) with axonemes (A) present in the peripheral cytoplasm. Scale bar = 1 µm. (**ii)** Enlargement of the enclosed area showing the details of a intranuclear spindle with microtubules with attach kinetochores (K) radiating from the nuclear poles (NP). Scale bar = 100nm.

Fig. 4: Spatiotemporal profile of NDC80-GFP expression during meiotic stages in the ookinete. (**A**) Live cell imaging of NDC80-GFP localization during various stage of ookinete development from zygote to mature ookinete in the mosquito gut (100x magnification). Merge: Hoechst (blue, DNA), GFP (green) and P28 (red, cell surface marker of activated female gamete, zygote and ookinete stages). Scale bar = 5 µM. (**B**) Ultrastructural analysis of kinetochore localization in a mature ookinete. (**i**) Longitudinal section through a mature ookinete showing the apical complex with several micronemes (M) and the more posterior nucleus (N). Scale bar = 1 µm. (**ii)** Enlargement of the nucleus showing the location of the four nuclear poles (arrows). Scale bar = 100 nm.

Fig. 5: NDC80-GFP localisation during oocyst development and sporozoite formation. (**A**) Live cell imaging of NDC80-GFP in oocysts at 7, 12, 14 and 21 days post-infection (dpi) and a sporozoite. Panels: DIC (differential interference contrast), Hoechst (blue, DNA), NDC80GFP (green, GFP), Merged: Hoechst (blue, DNA) and NDC80-GFP (green, GFP) Scale bar = 5µM. **(B)** Electron microscopy analysis of kinetochore location in an oocyst 12 day post-infection. **(i)** Central section through a mid-stage oocyst showing the early stages of sporozoite formation (S) at the surface of the oocyst cytoplasm. Scale bar = 10 µm. **(ii)** Detail showing the early stage in sporozoite budding. Note the underlying nucleus (N) with the nuclear pole and attached kinetochores (K) directed toward the budding sporozoite. R – Rhoptry anlagen. Scale bar = 100 nm.

Fig. 6: The NDC80 complex is conserved in *Plasmodium spp.* and most Apicomplexa **(A)** Domain composition of the four subunits of the NDC80 complex tetramer as commonly found in model eukaryotes. N and C denote the amino -and carboxy termini of the proteins. Numbers indicate the length in amino acids. **(B)** Mass spectrometry analysis of anti-GFP pulldowns of WT-GFP and NDC80-GFP from schizonts (8 hr culture) and gametocytes (activated for 1 min) stages. Numbers represent the total amount of peptides found per gene product. Colours correspond to panel A and indicate each of the four subunits of NDC80 complex. The previously unannotated gene PBANKA_1442300 is an SPC24 ortholog in *P. berghei* (see panel C). **(C)** *On the left:* presence/absence matrix of Ndc80 complex subunits in a large set of (newly sequenced) apicomplexan parasites, various Apicomplexa-affiliated lineages (outgroup e.g. chrompodellids) and a subset of eukaryotes. (see **Supplementary Table 3** for presence/absence table, and **Supplementary Sequence File 1** for sequences of

Ndc80 complex orthologs). Numbers indicate the average length of the orthologs in each collapsed clade represented in the phylogenetic tree. Note the consistently longer orthologs in Sarcocystidae (including *T. gondii*) and the expanded SPC24 ortholog in Plasmodiidae. *On the right:* workflow for the discovery of SPC24 orthologs in Hematozoa and Coccidia. Alignments represent RWD domains of putative SPC24 orthologs found using seed sequences (top: e.g. TGME49_212800). See **Fig. S5** for full alignments of RWD domains. The panels represent Hidden Markov Models (HMMs) of SPC24-like RWD domains, which were found to be significantly similar (see E-values) using HMM-vs-HMM search algorithm HHsearch (see methods).

Fig. S1:- Generation and genotype analysis of NDC80-GFP/mCherry parasite line. (A) Schematic representation of the endogenous *Ndc80*, the GFP/mCherry-tagging construct and the recombined *Ndc80* locus following single homologous recombination. Arrows 1, 2 and 3 indicate the position of PCR primers used to confirm successful integration of the construct. (B) Diagnostic PCR of NDC80-GFP and WTGFP parasites using primers IntT259 (NDC80, Arrow 1) and ol492 (for GFP line)/mCherry (for mCherry) (Arrow 3). IntT259 and T2592 (NDC80, Arrow 2) primers were used as control. Integration of the NDC80 tagging construct gives a band of 1269bp (GFP line) and 1335bp (mCherry line) for NDC80 parasite line. For controls, both WT and NDC80 tagged constructs gave a band size of 1153 bp. (C) Western blot of NDC80-GFP (96 kDa) and WT-GFP (29kDa) protein to illustrate the presence of intact NDC80-GFP in schizont stage extracts.

Fig. S2: Expression and location of NDC80-mCherry in asexual blood stages. Fluorescence was detected by live cell imaging. DIC: Differential interference contrast; Hoechst: blue, DNA; mCherry: red, NDC80-mCherry; Merge: Hoechst and mCherry fluorescence. Arrow shows doublets and arrow head shows singlet of Ndc80-mCherry. Scale bar = 5µM.

Fig. S3: Localization of *Plasmodium* NDC80-GFP in liver stages. Expression of the protein was detected in liver schizonts by live cell imaging. Merge = DAPI and GFP. Scale bar = 5 µM.

Fig. S4: NDC80 is not expressed in female gametocytes and gametes but shows centromeric location in male gametocytes. (A) Non-activated and activated gametocytes and gametes were examined by live cell imaging (100x magnification). DIC: differential interference contrast; Hoechst (blue, DNA), NDC80-GFP (green, GFP); P28 (red, cell surface marker of activated female gamete); Merge: Hoechst (blue, DNA), GFP (green) and P28 (red). **(B)** Male gametocytes treated with taxol (anti-tubulin inhibitor) at 1 min post activation showing location of NDC80. DMSO was used as control. **(C)** The location of

NDC80 (red) in relation to SMC4 (green), a kinetochore marker, in schizont and male gametocyte. **(D)** The location of NDC80 (green) in relation to kinesin-8B (red), an axonemal marker, in male gametocytes at 1 min- and 6 min- post activation. **(E)** Centromeric localization confirm by ChIP-seq analysis of NDC80-GFP profiles for all 14 chromosomes in gametocyte stage. Signals are plotted on a normalized read per million (RPM) basis.

Fig. S5: Full-length alignment of RWD domains of different SPC24 orthologs shown in Figure 6C. RWD domain alignment of SPC24 orthologs from our sequence database. Secondary structure of the three groups of orthologs (see Figure 6C) is based on the HHsearch algorithm. Colours and conservation metric are based on the clustal scheme as implemented in Jalview (Waterhouse et al., 2009)

Table legends:

Supplementary Table S1: Primers used in this study

Supplementary Table S2: Sources of genomes and transcripts of the sequence database used for sequence similarity searches including hyperlinks and/or reference to papers.

Supplementary Table S3: Presence/absence table of the Ndc80 complex (NDC80, NUF2, SPC25, SPC24). Absences are denoted by '-' and presences by the length of the ortholog.

Supplementary Sequence File 1: Orthologs of (including length per sequence in the FastA headers): *Pb*NDC80 (PBANKA_1115700), *Pb*NUF2 (PBANKA_0414300), *Pb*SPC25 (PBANKA_1358800), *Pb*SPC24 (PBANKA_1442300).

Video legends:

Supplementary Videos

SV1, SV2 and SV3: Three-dimensional visualization (3D rendered SIM Structured Illumination) of NDC80-GFP with respect to DAPI-stained nuclear DNA during early (SV1), middle (SV2) and late (SV3) stages of schizogony showing asynchronous division. Scale of the grid is 0.5 µm.

SV4: Time lapse video showing dynamics of NDC80-GFP during gametogony in 0-90 seconds. Scale bar = 5 µm.

SV5: Time lapse video showing dynamics of NDC80-GFP during gametogony in 90-180 seconds. Scale bar = 5 µm.

References

Akiyoshi, B., and K. Gull. 2013. Evolutionary cell biology of chromosome segregation: insights from trypanosomes. *Open Biol*. 3:130023.

Alushin, G.M., V.H. Ramey, S. Pasqualato, D.A. Ball, N. Grigorieff, A. Musacchio, and E. Nogales. 2010. The Ndc80 kinetochore complex forms oligomeric arrays along microtubules. *Nature*. 467:805-810.

Arnot, D.E., and K. Gull. 1998. The Plasmodium cell-cycle: facts and questions. *Ann Trop Med Parasitol*. 92:361-365.

Arnot, D.E., E. Ronander, and D.C. Bengtsson. 2011. The progression of the intra-erythrocytic cell cycle of Plasmodium falciparum and the role of the centriolar plaques in asynchronous mitotic division during schizogony. *Int J Parasitol*. 41:71-80.

Billker, O., V. Lindo, M. Panico, A.E. Etienne, T. Paxton, A. Dell, M. Rogers, R.E. Sinden, and H.R. Morris. 1998. Identification of xanthurenic acid as the putative inducer of malaria development in the mosquito. *Nature*. 392:289-292.

Bunnik, E.M., A. Venkat, J. Shao, K.E. McGovern, G. Batugedara, D. Worth, J. Prudhomme, S.A. Lapp, C. Andolina, L.S. Ross, L. Lawres, D. Brady, P. Sinnis, F. Nosten, D.A. Fidock, E.H. Wilson, R. Tewari, M.R. Galinski, C. Ben Mamoun, F. Ay, and K.G. Le Roch. 2019. Comparative 3D genome organization in apicomplexan parasites. *Proc Natl Acad Sci U S A*. 116:3183-3192.

Cheeseman, I.M. 2014. The kinetochore. *Cold Spring Harb Perspect Biol*. 6:a015826.

Ciferri, C., J. De Luca, S. Monzani, K.J. Ferrari, D. Ristic, C. Wyman, H. Stark, J. Kilmartin, E.D. Salmon, and A. Musacchio. 2005. Architecture of the human ndc80-hec1 complex, a critical constituent of the outer kinetochore. *J Biol Chem*. 280:29088-29095.

D'Archivio, S., and B. Wickstead. 2017. Trypanosome outer kinetochore proteins suggest conservation of chromosome segregation machinery across eukaryotes. *J Cell Biol*. 216:379-391.

Doerig, C., D. Chakrabarti, B. Kappes, and K. Matthews. 2000. The cell cycle in protozoan parasites. *Progress in cell cycle research*. 4:163-183.

Drechsler, H., and A.D. McAinsh. 2012. Exotic mitotic mechanisms. *Open Biol*. 2:120140.

Emms, D.M., and S. Kelly. 2019. OrthoFinder: phylogenetic orthology inference for comparative genomics. *Genome Biol*. 20:238.

Farrell, M., and M.J. Gubbels. 2014. The Toxoplasma gondii kinetochore is required for centrosome association with the centrocone (spindle pole). *Cell Microbiol*. 16:78-94.

Fennell, B.J., Z.A. Al-shatr, and A. Bell. 2008. Isotype expression, post-translational modification and stage-dependent production of tubulins in erythrocytic Plasmodium falciparum. *Int J Parasitol*. 38:527-539.

Ferguson, D.J., A.E. Balaban, E.M. Patzewitz, R.J. Wall, C.S. Hopp, B. Poulin, A. Mohmmed, P. Malhotra, A. Coppi, P. Sinnis, and R. Tewari. 2014. The repeat region of the circumsporozoite protein is critical for sporozoite formation and maturation in Plasmodium. *PLoS One*. 9:e113923.

Ferguson, D.J., F.L. Henriquez, M.J. Kirisits, S.P. Muench, S.T. Prigge, D.W. Rice, C.W. Roberts, and R.L. McLeod. 2005. Maternal inheritance and stage-specific variation of the apicoplast in Toxoplasma gondii during development in the intermediate and definitive host. *Eukaryot Cell*. 4:814-826.

Ferguson, D.J.P., N. Sahoo, R.A. Pinches, J.M. Bumstead, F.M. Tomley, and M.-J. Gubbels. 2008. MORN1 has a conserved role in asexual and sexual development across the apicomplexa. *Eukaryotic cell*. 7:698-711.

Francia, M.E., J.F. Dubremetz, and N.S. Morrissette. 2015. Basal body structure and composition in the apicomplexans Toxoplasma and Plasmodium. *Cilia*. 5:3.

Francia, M.E., and B. Striepen. 2014. Cell division in apicomplexan parasites. *Nat Rev Microbiol*. 12:125-136.

Gerald, N., B. Mahajan, and S. Kumar. 2011. Mitosis in the human malaria parasite Plasmodium falciparum. *Eukaryot Cell*. 10:474-482.

Guttery, D.S., M. Roques, A.A. Holder, and R. Tewari. 2015. Commit and Transmit: Molecular Players in Plasmodium Sexual Development and Zygote Differentiation. *Trends in parasitology*. 31:676-685.

Hoeijmakers, W.A., C. Flueck, K.J. Francoijs, A.H. Smits, J. Wetzel, J.C. Volz, A.F. Cowman, T. Voss, H.G. Stunnenberg, and R. Bartfai. 2012. Plasmodium falciparum centromeres display a unique epigenetic makeup and cluster prior to and during schizogony. *Cell Microbiol*. 14:1391-1401.

Iwanaga, S., S.M. Khan, I. Kaneko, Z. Christodoulou, C. Newbold, M. Yuda, C.J. Janse, and A.P. Waters. 2010. Functional identification of the Plasmodium centromere and generation of a Plasmodium artificial chromosome. *Cell Host Microbe*. 7:245-255.

Janouskovec, J., G.G. Paskerova, T.S. Miroliubova, K.V. Mikhailov, T. Birley, V.V. Aleoshin, and T.G. Simdyanov. 2019. Apicomplexan-like parasites are polyphyletic and widely but selectively dependent on cryptic plastid organelles. *Elife*. 8.

Janouskovec, J., D.V. Tikhonenkov, F. Burki, A.T. Howe, M. Kolisko, A.P. Mylnikov, and P.J. Keeling. 2015. Factors mediating plastid dependency and the origins of parasitism in apicomplexans and their close relatives. *Proc Natl Acad Sci U S A*. 112:10200-10207.

Janse, C.J., B. Franke-Fayard, G.R. Mair, J. Ramesar, C. Thiel, S. Engelmann, K. Matuschewski, G.J. van Gemert, R.W. Sauerwein, and A.P. Waters. 2006. High efficiency transfection of Plasmodium berghei facilitates novel selection procedures. *Mol Biochem Parasitol*. 145:60-70.

Janse, C.J., T. Ponnudurai, A.H. Lensen, J.H. Meuwissen, J. Ramesar, M. Van der Ploeg, and J.P. Overdulve. 1988. DNA synthesis in gametocytes of Plasmodium falciparum. *Parasitology*. 96 (Pt 1):1-7.

Johnson, L.S., S.R. Eddy, and E. Portugaly. 2010. Hidden Markov model speed heuristic and iterative HMM search procedure. *BMC Bioinformatics*. 11:431.

Katoh, K., and D.M. Standley. 2013. MAFFT multiple sequence alignment software version 7: improvements in performance and usability. *Mol Biol Evol*. 30:772-780.

Komaki-Yasuda, K., M. Okuwaki, K. Nagata, S. Kawazu, and S. Kano. 2013. Identification of a novel and unique transcription factor in the intraerythrocytic stage of Plasmodium falciparum. *PLoS One*. 8:e74701.

Mathur, V., M. Kolisko, E. Hehenberger, N.A.T. Irwin, B.S. Leander, A. Kristmundsson, M.A. Freeman, and P.J. Keeling. 2019. Multiple Independent Origins of Apicomplexan-Like Parasites. *Curr Biol*. 29:2936-2941 e2935.

McKinley, K.L., and I.M. Cheeseman. 2016. The molecular basis for centromere identity and function. *Nat Rev Mol Cell Biol*. 17:16-29.

Munoz-Gomez, S.A., K. Durnin, L. Eme, C. Paight, C.E. Lane, M.B. Saffo, and C.H. Slamovits. 2019. Nephromyces Represents a Diverse and Novel Lineage of the Apicomplexa That Has Retained Apicoplasts. *Genome Biol Evol*. 11:2727-2740.

Musacchio, A., and A. Desai. 2017. A Molecular View of Kinetochore Assembly and Function. *Biology (Basel)*. 6.

Pandey, R., S. Abel, M. Boucher, R.J. Wall, M. Zeeshan, E. Rea, A. Freville, X.M. Lu, D. Brady, E. Daniel, R.R. Stanway, S. Wheatley, G. Batugedara, T. Hollin, A.R. Bottrill, D. Gupta, A.A. Holder, K.G. Le Roch, and R. Tewari. 2019. Plasmodium condensin core subunits (SMC2/SMC4) mediate atypical mitosis and are essential for parasite proliferation and transmission. *bioRxiv*.

Petrovic, A., J. Keller, Y. Liu, K. Overlack, J. John, Y.N. Dimitrova, S. Jenni, S. van Gerwen, P. Stege, S. Wohlgemuth, P. Rombaut, F. Herzog, S.C. Harrison, I.R. Vetter, and A. Musacchio. 2016. Structure of the MIS12 Complex and Molecular Basis of Its Interaction with CENP-C at Human Kinetochores. *Cell*. 167:1028-1040 e1015.

Richmond, D., R. Rizkallah, F. Liang, M.M. Hurt, and Y. Wang. 2013. Slk19 clusters kinetochores and facilitates chromosome bipolar attachment. *Mol Biol Cell*. 24:566-577.

Roques, M., R.R. Stanway, E.I. Rea, R. Markus, D. Brady, A.A. Holder, D.S. Guttery, and R. Tewari. 2019. Plasmodium centrin PbCEN-4 localizes to the putative MTOC and is dispensable for malaria parasite proliferation. *Biol Open*. 8.

Saini, E., M. Zeeshan, D. Brady, R. Pandey, G. Kaiser, L. Koreny, P. Kumar, V. Thakur, S. Tatiya, N.J. Katris, R.S. Limenitakis, I. Kaur, J.L. Green, A.R. Bottrill, D.S. Guttery, R.F. Waller, V. Heussler, A.A. Holder, A. Mohmmed, P. Malhotra, and R. Tewari. 2017. Photosensitized INA-Labelled protein 1 (PhIL1) is novel component of the inner membrane complex and is required for Plasmodium parasite development. *Sci Rep*. 7:15577.

Schrevel, J., G. Asfaux-Foucher, and J.M. Bafort. 1977. [Ultrastructural study of multiple mitoses during sporogony of Plasmodium b. berghei]. *J Ultrastruct Res*. 59:332-350.

Sezen, B., M. Seedorf, and E. Schiebel. 2009. The SESA network links duplication of the yeast centrosome with the protein translation machinery. *Genes Dev*. 23:1559-1570.

Sinden, R.E. 1983. Sexual development of malarial parasites. *Adv Parasitol*. 22:153-216.

Sinden, R.E. 1991a. Asexual blood stages of malaria modulate gametocyte infectivity to the mosquito vector--possible implications for control strategies. *Parasitology*. 103 Pt 2:191-196.

Sinden, R.E. 1991b. Mitosis and meiosis in malarial parasites. *Acta Leiden*. 60:19-27.

Sinden, R.E., E.U. Canning, R.S. Bray, and M.E. Smalley. 1978. Gametocyte and gamete development in Plasmodium falciparum. *Proc R Soc Lond B Biol Sci*. 201:375-399.

Sinden, R.E., E.U. Canning, and B. Spain. 1976. Gametogenesis and fertilization in Plasmodium yoelii nigeriensis: a transmission electron microscope study. *Proc R Soc Lond B Biol Sci*. 193:55-76.

Sinden, R.E., A. Talman, S.R. Marques, M.N. Wass, and M.J. Sternberg. 2010. The flagellum in malarial parasites. *Curr Opin Microbiol*. 13:491-500.

Solovei, I., L. Schermelleh, K. During, A. Engelhardt, S. Stein, C. Cremer, and T. Cremer. 2004. Differences in centromere positioning of cycling and postmitotic human cell types. *Chromosoma*. 112:410-423.

Steinegger, M., M. Meier, M. Mirdita, H. Vohringer, S.J. Haunsberger, and J. Soding. 2019. HH-suite3 for fast remote homology detection and deep protein annotation. *BMC Bioinformatics*. 20:473.

Sundin, L.J., G.J. Guimaraes, and J.G. Deluca. 2011. The NDC80 complex proteins Nuf2 and Hec1 make distinct contributions to kinetochore-microtubule attachment in mitosis. *Mol Biol Cell*. 22:759-768.

Suvorova, E.S., M. Francia, B. Striepen, and M.W. White. 2015. A novel bipartite centrosome coordinates the apicomplexan cell cycle. *PLoS Biol*. 13:e1002093.

Swedlow, J.R., K. Hu, P.D. Andrews, D.S. Roos, and J.M. Murray. 2002. Measuring tubulin content in Toxoplasma gondii: a comparison of laser-scanning confocal and wide-field fluorescence microscopy. *Proceedings of the National Academy of Sciences of the United States of America*. 99:2014-2019.

Tewari, R., D. Dorin, R. Moon, C. Doerig, and O. Billker. 2005. An atypical mitogen-activated protein kinase controls cytokinesis and flagellar motility during male gamete formation in a malaria parasite. *Mol Microbiol*. 58:1253-1263.

Tewari, R., U. Straschil, A. Bateman, U. Bohme, I. Cherevach, P. Gong, A. Pain, and O. Billker. 2010. The systematic functional analysis of Plasmodium protein kinases identifies essential regulators of mosquito transmission. *Cell Host Microbe*. 8:377-387.

Tromer, E.C., J.J.E. van Hooff, G. Kops, and B. Snel. 2019. Mosaic origin of the eukaryotic kinetochore. *Proc Natl Acad Sci U S A*. 116:12873-12882.

Vader, G., and A. Musacchio. 2017. The greatest kinetochore show on earth. *EMBO Rep*. 18:1473-1475.

Vaishnava, S., D.P. Morrison, R.Y. Gaji, J.M. Murray, R. Entzeroth, D.K. Howe, and B. Striepen. 2005. Plastid segregation and cell division in the apicomplexan parasite Sarcocystis neurona. *J Cell Sci*. 118:3397-3407.

van Hooff, J.J., E. Tromer, L.M. van Wijk, B. Snel, and G.J. Kops. 2017. Evolutionary dynamics of the kinetochore network in eukaryotes as revealed by comparative genomics. *EMBO Rep*. 18:1559-1571.

Verma, G., and N. Surolia. 2013. Plasmodium falciparum CENH3 is able to functionally complement Cse4p and its, C-terminus is essential for centromere function. *Mol Biochem Parasitol*. 192:21-29.

Verma, G., and N. Surolia. 2014. The dimerization domain of PfCENP-C is required for its functions as a centromere protein in human malaria parasite Plasmodium falciparum. *Malar J*. 13:475.

Waterhouse, A.M., J.B. Procter, D.M. Martin, M. Clamp, and G.J. Barton. 2009. Jalview Version 2--a multiple sequence alignment editor and analysis workbench. *Bioinformatics*. 25:1189-1191.

Wei, R.R., P.K. Sorger, and S.C. Harrison. 2005. Molecular organization of the Ndc80 complex, an essential kinetochore component. *Proc Natl Acad Sci U S A*. 102:5363-5367.

Westermann, S., D.G. Drubin, and G. Barnes. 2007. Structures and functions of yeast kinetochore complexes. *Annu Rev Biochem*. 76:563-591.

WHO. 2018. World malaria report 2018. *World Health Organization*.

Zeeshan, M., D.J. Ferguson, S. Abel, A. Burrrell, E. Rea, D. Brady, E. Daniel, M. Delves, S. Vaughan, A.A. Holder, K.G. Le Roch, C.A. Moores, and R. Tewari. 2019a. Kinesin-8B controls basal body function and flagellum formation and is key to malaria transmission. *Life Sci Alliance*. 2.

Zeeshan, M., F. Shilliday, T. Liu, S. Abel, T. Mourier, D.J.P. Ferguson, E. Rea, R.R. Stanway, M. Roques, D. Williams, E. Daniel, D. Brady, A.J. Roberts, A.A. Holder, A. Pain, K.G. Le Roch, C.A. Moores, and R. Tewari. 2019b. Plasmodium kinesin-8X associates with mitotic spindles and is essential for oocyst development during parasite proliferation and transmission. *PLoS Pathog*. 15:e1008048.

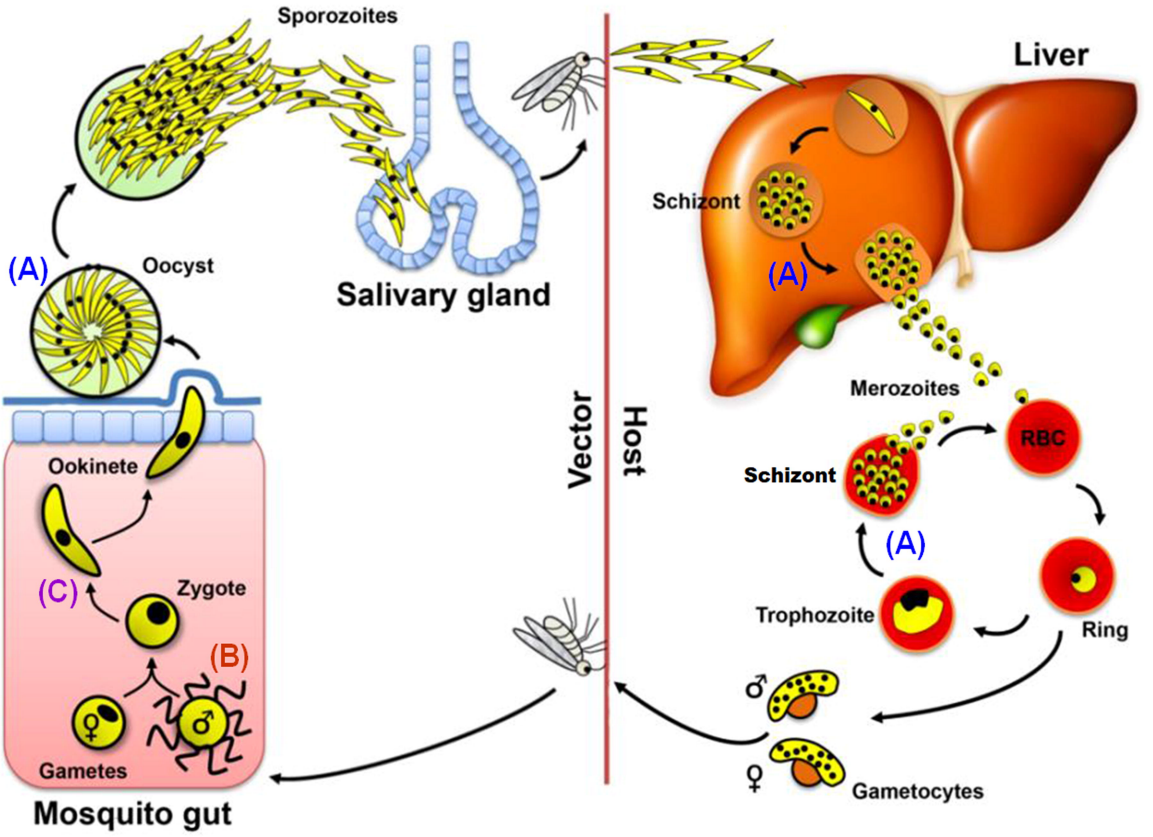

A- Endomitotic division (Schizogony- schizont formation in the mammalian liver and blood cells and sporogony (sporozoite formation) in the mosquito gut. B- endoreduplication (Male gametogenesis in mosquito gut). C- Meiotic cell division (zygote to ookinete differentiation in the mosquito gut)

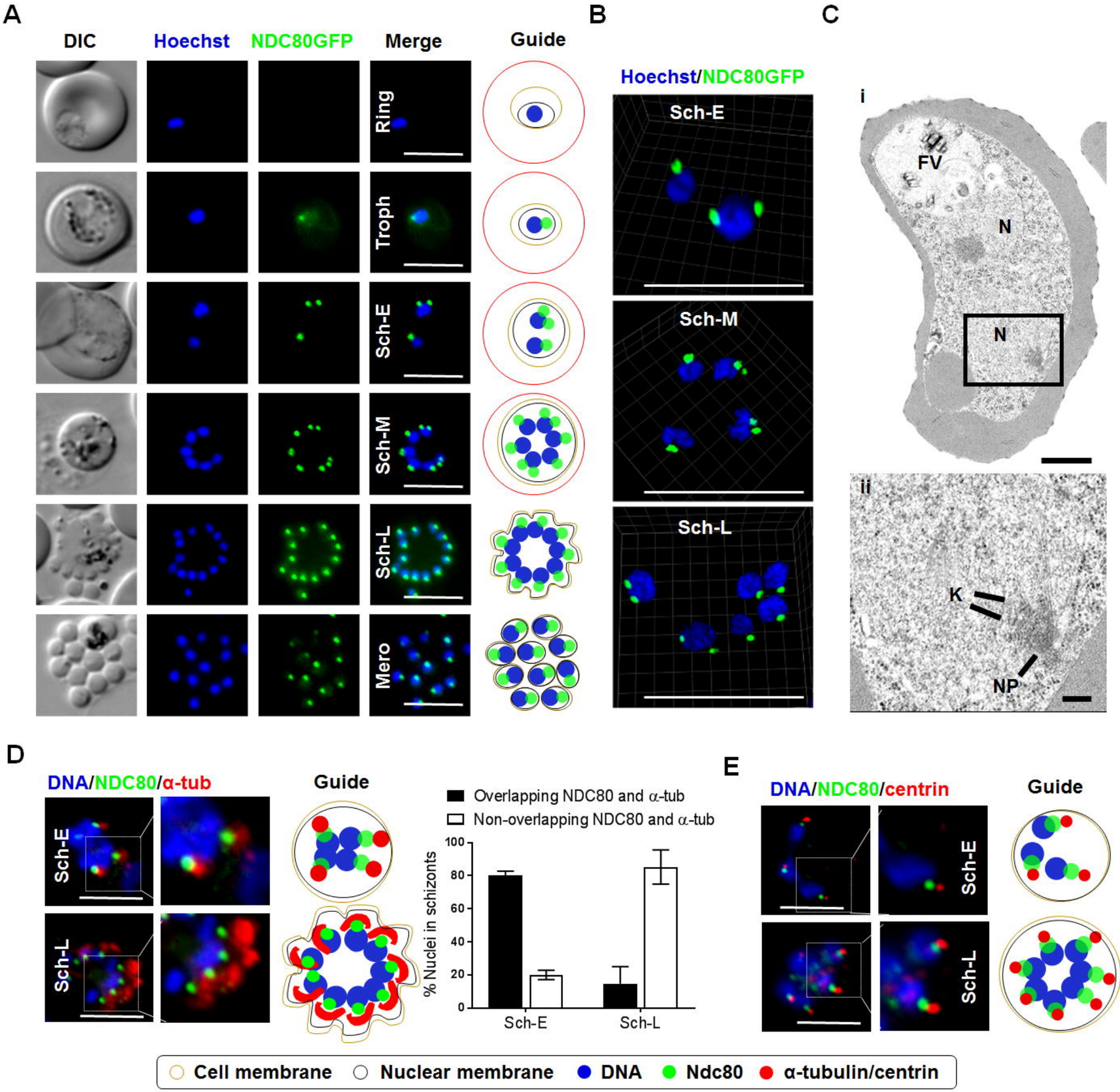
A
DIC
Hoechst
NDC80GFP
Merge
Guide
Ring
Troph
Sch-E
Sch-M
Sch-L
Mero
B
Hoechst/NDC80GFP
Sch-E
Sch-M
Sch-L
C
i
FV
N
N
ii
K
NP
D
DNA/NDC80/α-tub
Guide
Sch-E
Sch-L
Overlapping NDC80 and α-tub
Non-overlapping NDC80 and α-tub
% Nuclei in schizonts
100
80
60
40
20
0
Sch-E
Sch-L
E
DNA/NDC80/centrin
Guide
Sch-E
Sch-L
Cell membrane
Nuclear membrane
DNA
Ndc80
α-tubulin/centrin

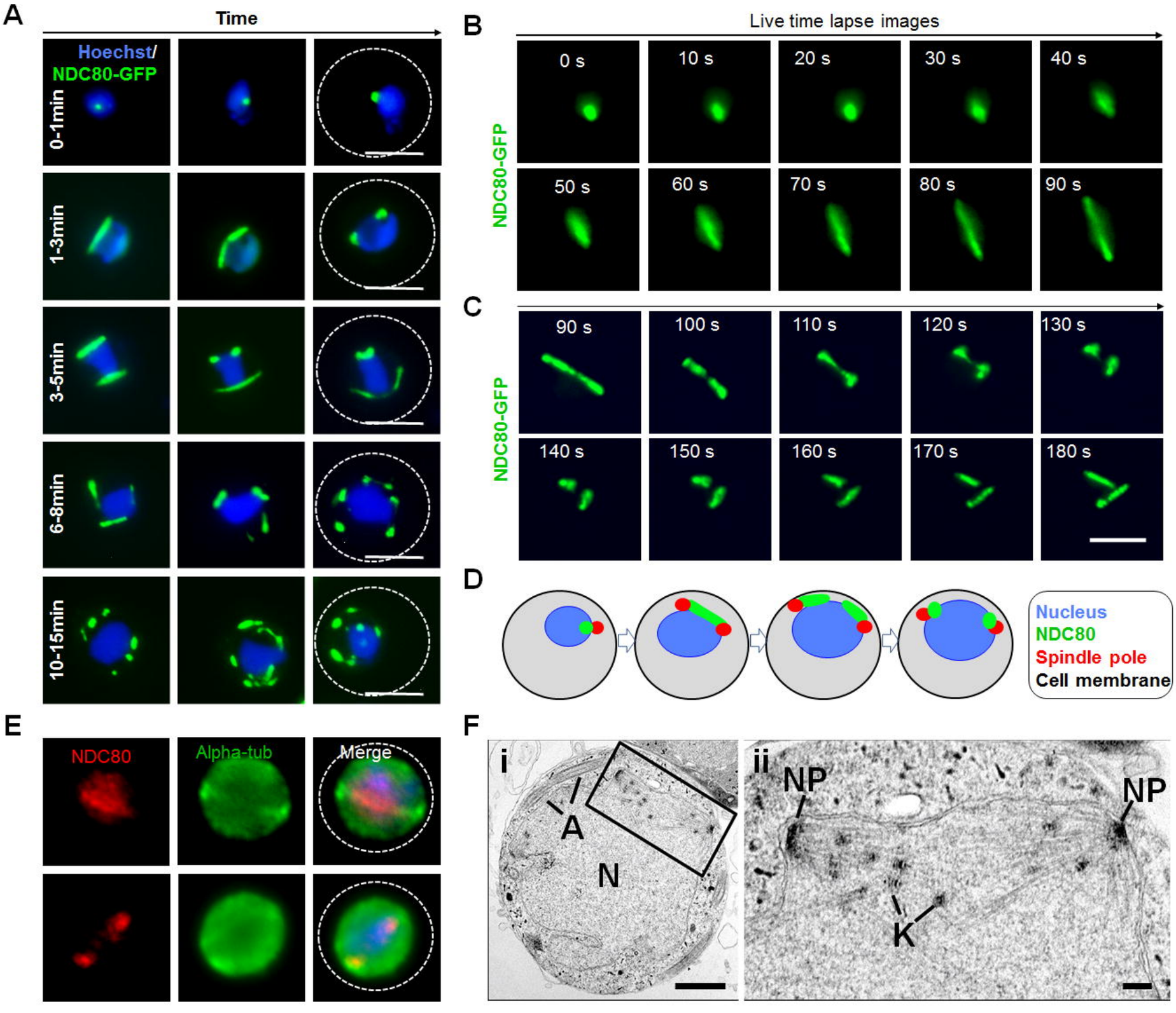
A
Time
Hoechst/
NDC80-GFP
0-1min
1-3min
3-5min
6-8min
10-15min
B
Live time lapse images
NDC80-GFP
0 s
10 s
20 s
30 s
40 s
50 s
60 s
70 s
80 s
90 s
C
NDC80-GFP
90 s
100 s
110 s
120 s
130 s
140 s
150 s
160 s
170 s
180 s
D
Nucleus
NDC80
Spindle pole
Cell membrane
E
NDC80
Alpha-tub
Merge
F
i
A
N
ii
NP
NP
K

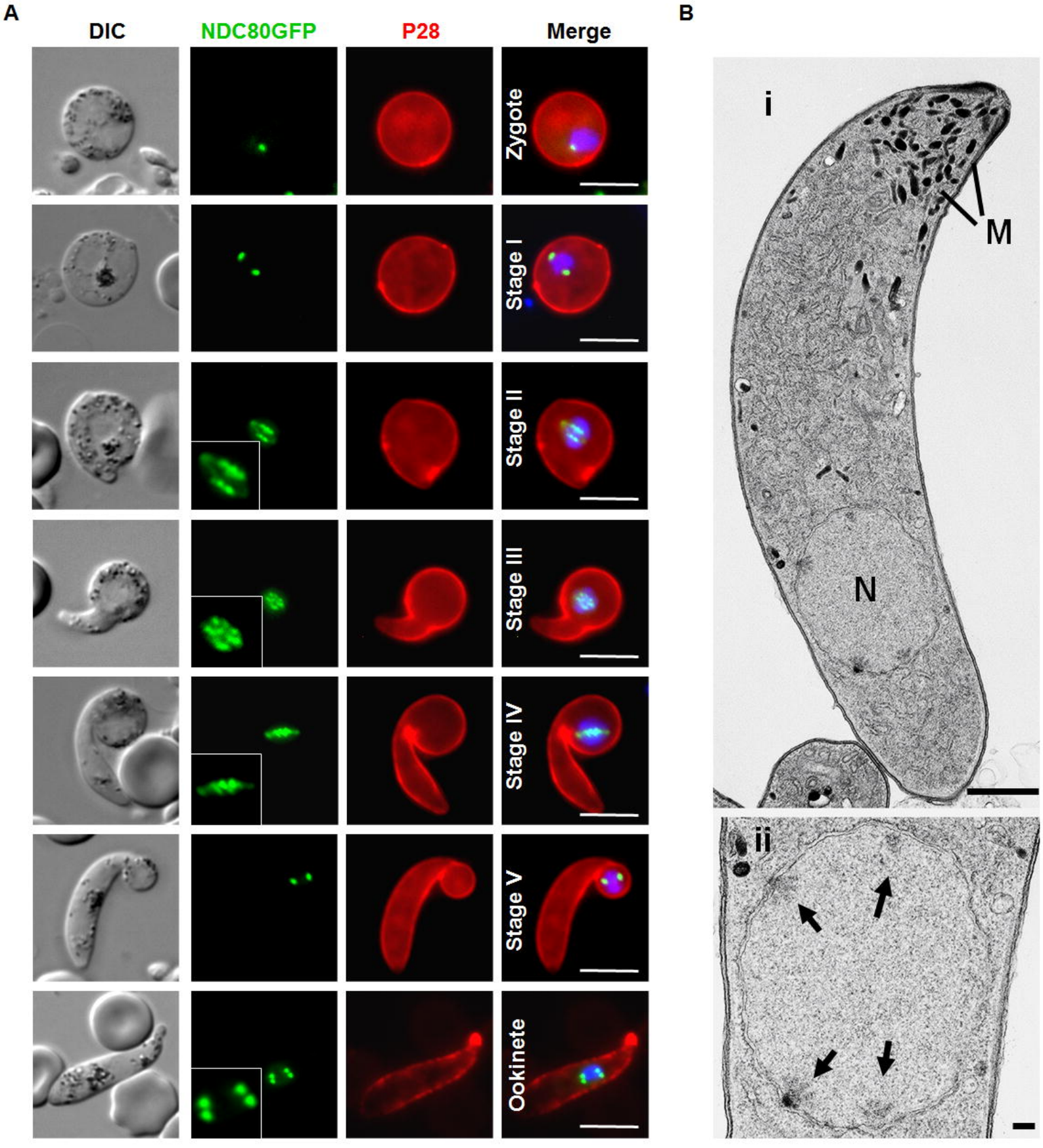
A
DIC
NDC80GFP
P28
Merge
Zygote
Stage I
Stage II
Stage III
Stage IV
Stage V
Ookinete
B
i
M
N
ii

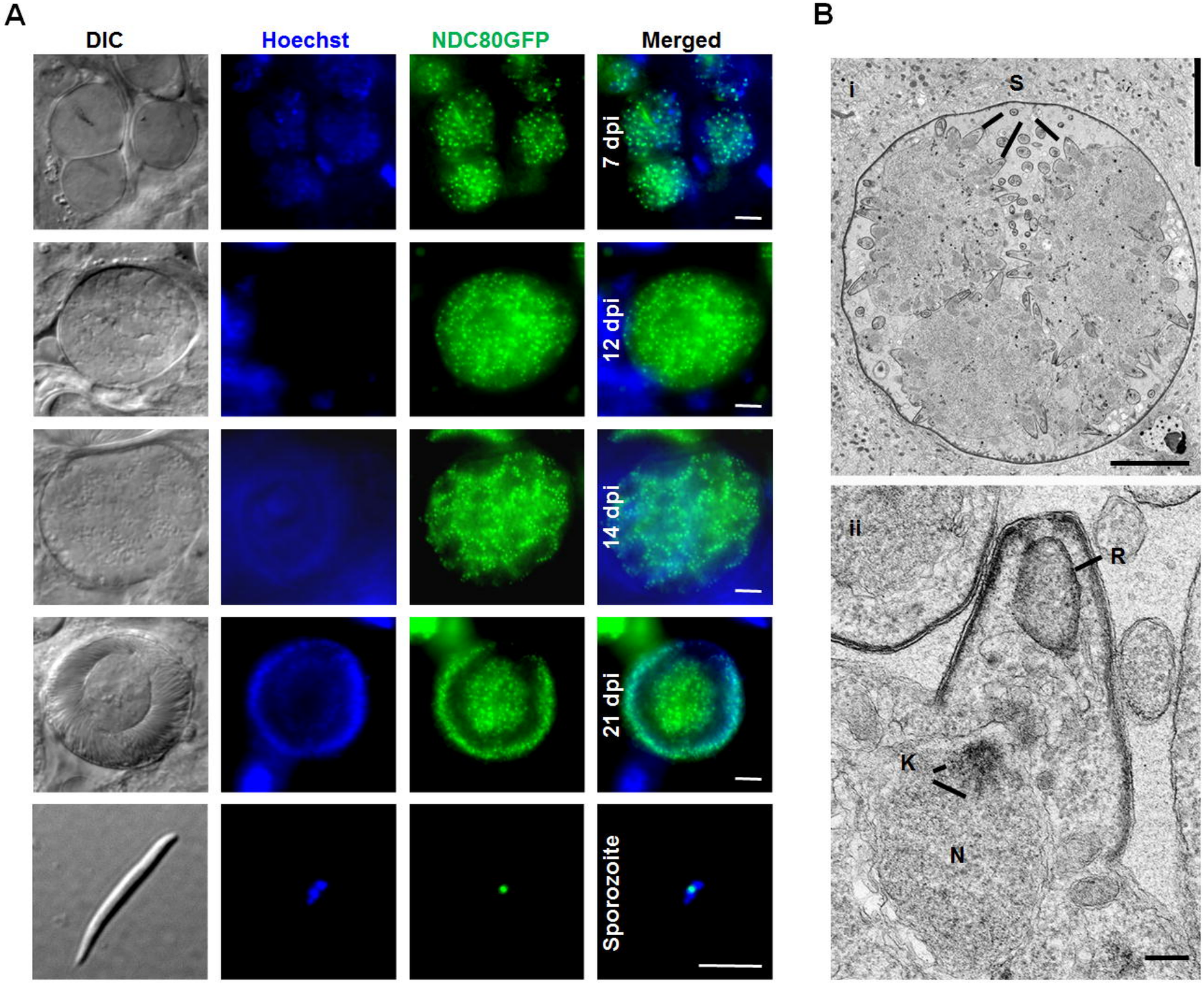
A
DIC
Hoechst
NDC80GFP
Merged
7 dpi
12 dpi
14 dpi
21 dpi
Sporozoite
B
i
S
ii
R
K
N

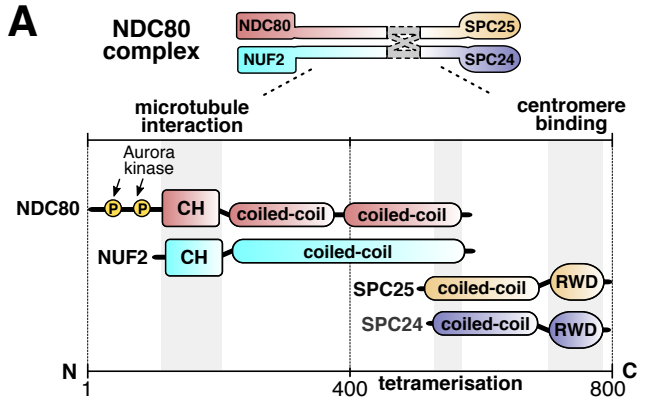

B
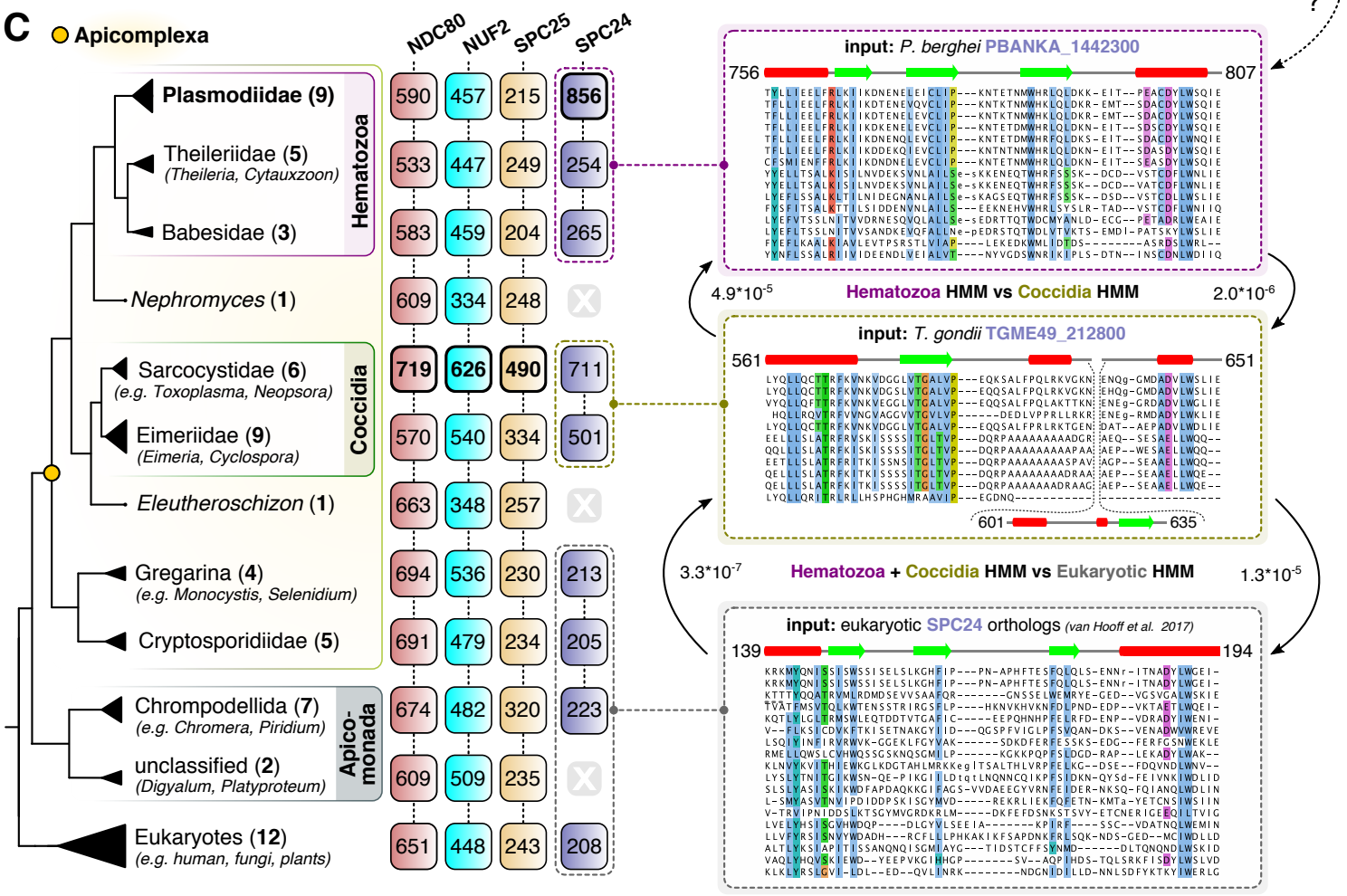
P. berghei gene ID	product description *function*	length (aa)	schizonts GFP	schizonts NDC80 GFP		gametocytes GFP	gametocytes NDC80 GFP	
PBANKA_1115700	**kinetochore protein NDC80** *microtubule attachment*	**589**	**0**	**29**	**22**	**0**	**22**	**21**
PBANKA_0414300	**kinetochore protein NUF2** *microtubule attachment*	**457**	**0**	**18**	**14**	**0**	**6**	**16**
PBANKA_1210200	PRE-binding protein *transcription*	970	0	9	8	0	0	4
PBANKA_1116800	conserved protein *unknown function*	448	0	5	5	0	0	3
PBANKA_1358800	**kinetochore protein SPC25** *microtubule attachment*	**216**	**0**	**2**	**5**	**0**	**0**	**4**
PBANKA_1442300	**conserved Plasmodium protein** *unknown function*	**819**	**0**	**2**	**4**	**0**	**0**	**4**
PBANKA_1458300	kinesin-13 *microtubule depolymerisation*	1025	0	0	0	0	0	2